NAVAL POSTGRADUATE SCHOOL
Monterey, California

DTIC
ELECTE
FEB 0 6 1992
B
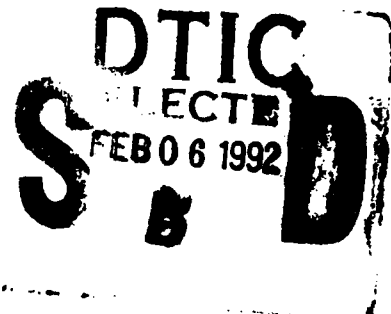
THESIS

FACTORS INFLUENCING THE MICROSTRUCTURAL
AND MECHANICAL PROPERTIES OF
ULCB STEEL WELDMENTS

by

Paul F. McHale

December, 1991

Thesis Advisor: Alan G. Fox

Approved for public release; distribution is unlimited.

92-03148

SECURITY CLASSIFICATION OF THIS PAGE

REPORT DOCUMENTATION PAGE

1a REPORT SECURITY CLASSIFICATION UNCLASSIED	1b RESTRICTIVE MARKINGS
2a. SECURITY CLASSIFICATION AUTHORITY	3 DISTRIBUTION/AVAILABILITY OF REPORT
2b. DECLASSIFICATION/DOWNGRADING SCHEDULE	Approved for public release; distribution is unlimited.

4 PERFORMING ORGANIZATION REPORT NUMBER(S)	5. MONITORING ORGANIZATION REPORT NUMBER(S)

6a NAME OF PERFORMING ORGANIZATION Naval Postgraduate School	6b. OFFICE SYMBOL (If applicable) ME	7a. NAME OF MONITORING ORGANIZATION Naval Postgraduate School
6c ADDRESS (City, State, and ZIP Code) Monterey, CA 93943-5000		7b ADDRESS (City, State, and ZIP Code) Monterey, CA 93943-5000

8a. NAME OF FUNDING/SPONSORING ORGANIZATION David Taylor Research Center	8b. OFFICE SYMBOL (If applicable) Code 2814	9. PROCUREMENT INSTRUMENT IDENTIFICATION NUMBER
8c. ADDRESS (City, State, and ZIP Code) Annapolis, MD 21402		10 SOURCE OF FUNDING NUMBERS

Program Element No	Project No	Task No	Work Unit Accession Number

11. TITLE (Include Security Classification)
FACTORS INFLUENCING THE MICROSTRUCTURAL AND MECHANICAL PROPERTIES OF ULCB STEEL WELDMENTS

12. PERSONAL AUTHOR(S) Paul Francis McHale

13a TYPE OF REPORT Master's Thesis	13b TIME COVERED From To	14. DATE OF REPORT (year, month, day) December 1991	15 PAGE COUNT 104

16 SUPPLEMENTARY NOTATION
The views expressed in this thesis are those of the author and do not reflect the official policy or position of the Department of Defense or the U.S. Government.

17. COSATI CODES			18. SUBJECT TERMS (continue on reverse if necessary and identify by block number)
FIELD	GROUP	SUBGROUP	Ultra Low Carbon Bainitic steel
			Nonmetallic inclusions
			Constitutional supercooling

19. ABSTRACT (continue on reverse if necessary and identify by block number)

The U.S. Navy has maintained a continuous research, development and certification program in HSLA and ULCB steels as a replacement for the HY steels used in ship construction. The major benefit of the HSLA and ULCB steels stems from the relative ease of weldability as compared with the HY steels which require large amounts of preheating to prevent weld metal crack formation. This study focused on ULCB steel weldment mechanical properties which were shown to be largely dependent on the heat input and to a lesser extent the base plate composition, cover gas and nonmetallic inclusion composition and content. The heat input rate and subsequent cooling rate for the ULCB/ULCB steel weldments determined the degree of constitutional supercooling indicating a high heat input (large constitutional supercooling) resulted in a tough, finely grained macrostructure while the lower heat input (small constitutional supercooling) generated a weak, columnar/dendritic macrostructure. The utilization of HY-130 base metal resulted in increased carbon pickup in the fusion zone and consequently poorer mechanical properties. The use of a reactive cover gas markedly increased the inclusion density and promoted the formation of carbides producing the poorest overall mechanical properties. The majority of the nonmetallic inclusions identified were spherical, complex aluminum-silicates or manganese-aluminum-silicates. The presence of inclusions did not appear to be dominant in the nucleation of acicular ferrite or in controlling the microstructural development.

20 DISTRIBUTION/AVAILABILITY OF ABSTRACT	21 ABSTRACT SECURITY CLASSIFICATION
☒ UNCLASSIFIED/UNLIMITED ☐ SAME AS REPORT ☐ DTIC USERS	Unclassified
22a. NAME OF RESPONSIBLE INDIVIDUAL Alan G. Fox	22b TELEPHONE (Include Area code) (408) 646-2142	22c OFFICE SYMBOL ME/Fx

DD FORM 1473, 84 MAR   83 APR edition may be used until exhausted   SECURITY CLASSIFICATION OF THIS PAGE
All other editions are obsolete   Unclassifeid

i

Factors Influencing The Microstructural

And Mechanical Properties Of

ULCB Steel Weldments

by

Paul F. McHale

Lieutenant, United States Navy

B.S.M.E., United States Naval Academy, 1985

Submitted in partial fulfillment

of the requirements for the degree of

MASTER OF SCIENCE IN MECHANICAL ENGINEERING

from the

NAVAL POSTGRADUATE SCHOOL

December 1991

Author: _____
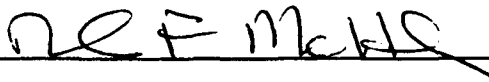
Paul F. McHale

Approved by: _____

Alan G. Fox,, Thesis Advisor

_____
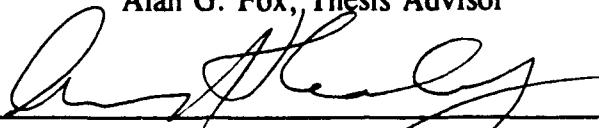
Anthony J. Healey, Chairman

Department of Mechanical Engineering

ii

ABSTRACT

The U.S. Navy has maintained a continuous research, development and certification program in HSLA and ULCB steels as a replacement for the HY steels used in ship construction. The major benefit of the HSLA and ULCB steels stems from the relative ease of weldability as compared with the HY steels which require large amounts of preheating to prevent weld metal crack formation. This study focused on ULCB steel weldment mechanical properties which were shown to be largely dependent on the heat input and to a lesser extent the base plate composition, cover gas and nonmetallic inclusion composition and content. The heat input rate and subsequent cooling rate for the ULCB/ULCB steel weldments determined the degree of constitutional supercooling indicating a high heat input (large constitutional supercooling) resulted in a tough, finely grained macrostructure while the lower heat input (small constitutional supercooling) generated a weak, columnar/dendritic macrostructure. The utilization of HY-130 base metal resulted in increased carbon pickup in the fusion zone and consequently poorer mechanical properties. The use of a reactive cover gas markedly increased the inclusion density and promoted the formation of carbides producing the poorest overall mechanical properties. The majority of the nonmetallic inclusions identified were spherical, complex aluminum-silicates or manganese-aluminum-silicates. The presence of inclusions did not appear to be dominant in the nucleation of acicular ferrite or in controlling the microstructural development.

TABLE OF CONTENTS

LIST OF FIGURES

ACKNOWLEDGEMENTS

I. INTRODUCTION

The development of High Strength Low Alloy (HSLA) and Ultra Low Carbon

Bainitic (ULCB) steels as an alternative to High Yield (HY) steels correlates directly into

construction of submarines that will submerge to greater operating depths and operate at

higher speeds. This can be accomplished only with a steel that is stronger and tougher

yielding reduced weight (speed) and the ability to withstand greater submergence pressure

(depth). For the past decade the U.S. Navy has maintained a continuous research,

development and certification program in HSLA steels to replace the use of HY steels

for hull construction. HSLA and ULCB steels improve productivity and reduce hull

fabrication cost largely by reducing or eliminating the need ior preheating HY-80, HY-

100 and HY-130 steels prior to welding. Long hours of preheating HY steels is required

to prevent weld-metal crack formation (Irving, 1987, p.34). Ultra Low Carbon Bainitic

(ULCB) steel is a relatively new family of steels which has the metallurgical attributes

ideal for the development of a high strength, high toughness weld metal. The ultimate

benefit of ULCB steel weld metal is achieved in conjunction with the use of HSLA-130

low carbon base metal to minimize the potential for weld metal carbon pickup (Gudas,

1989, p.8).

The size, distribution and chemical composition of nonmetallic inclusions in steel

weldments greatly influences the strength and toughness. Large inclusions act in a

detrimental manner as fracture initiation sites. Small inclusions ($< 1\mu$m) may be used

1

to control the microstructure of the weld metal and HAZ regions resulting in improved toughness. Of particular interest is the role of nonmetallic inclusions in the nucleation of acicular ferrite. Acicular ferrite is the microstructural constituent which produces a desirable high resistance to cleavage and thus improved metal toughness (Kiessling, 1989, p.104).

This study investigated the size, distribution and chemical composition of non-metallic inclusions in ultra low carbon steel weldments in both ULCB and HY parent metal and the effect of these inclusions on the weld metal microstructures and toughness. TIG and MIG weldments were evaluated at varying heat input rates. Small amounts of oxygen and carbon dioxide added to shielding gases aid in arc stabilization. The effect of such reactive shielding gases was established.

II. BACKGROUND

A. HIGH YIELD AND HIGH STRENGTH LOW ALLOY STEELS

High Yield (HY) steels use the traditional quench and temper method to achieve weld metal with strength >690MPa (100ksi). Carbon and other alloying elements such as Ni, Cr, Mn and Mo are utilized for strengthening and to achieve the required hardenability. Welding of HY steels places significant restrictions on welding heat input, plate thickness and interpass temperature as well as requiring large amounts of preheat. The quenched and tempered HY steel requires a high cooling rate in the weld to achieve the desired strength thereby restricting the maximum heat input. The maximum heat input is further restricted due to the high susceptibility of the quench and tempered martensitic microstructure to hydrogen induced cold cracking (HIC). Costly and extensive preheating is required to prevent cold cracking in HY steels. (Gudas, 1989, p.8)

The past decade has seen extensive research in the development of High Strength Low Alloy (HSLA) steels as a suitable substitute for the HY steels. HSLA steels reduce hull fabrication costs largely due to the minimization or elimination of preheat for welding and are less susceptible to HIC. HSLA steels are low carbon, copper precipitation strengthened steels which also involve controlled rolling and thermomechanical treatment to attain the desired strengths. The strengthening mechanisms utilized in HSLA steels include grain refinement, precipitation strengthening,

3

solid solution strengthening and the formation of dislocation substructures produced by deformation processing and bainitic/martensitic phase transformation (Coldren, Cox, 1986, p.3). HSLA-80 steel is certified and currently in use for CG-47, DDG-51, CVN-68 and LHD-1 class ship construction (Gudas, 1989, p.3). HSLA-100 steel incorporates increased copper content over HSLA-80 steels for more precipitation strengthening and higher levels of Mn, Ni, Mo and Cu for improved hardenability (Czyryca, Link, 1988, p.3). The progressive development of HY and HSLA steels has resulted in carbon contents being lowered to below 0.10 weight percent carbon. The Graville diagram (See Figure 1) illustrates that steels with low carbon content are more resistant to cold cracking over the entire range of carbon equivalent values (CEV). The CEV is a measure of the metal's ability to resist hydrogen induced cracking. The low carbon steels fall into Zone I and are easily weldable under all conditions whereas the HY steels have significant carbon content and large alloying additions making them more difficult to weld since they are much more susceptible to HIC.

Graville Diagram

$$CE = C + \frac{Mn+Si}{6} + \frac{Ni+Cu}{15} + \frac{Cr+Mo+V}{5}$$
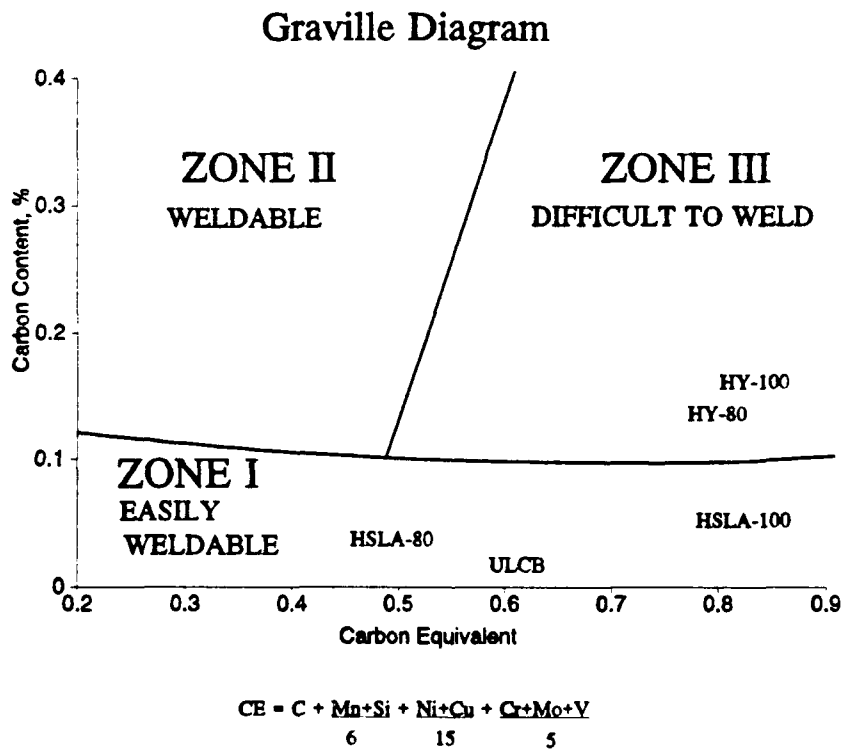
Figure 1

Graville diagram illustrating the relative ease of weldability for HY, HSLA and ULCB steels (Blicharski et al., 1988, p.318).

5

B. ULTRA LOW CARBON BAINITIC STEEL

Ultra Low Carbon Bainitic steel serves as an alternative to the traditional method (quench and temper of higher carbon steels) of developing a weld metal with yield strength above 690MPa (100 ksi). ULCB steels obtain their high strength and high resistance to both ductile and brittle fracture through alloy design and advanced thermomechanical processing. Their strength is derived from dislocation substructures and solid solution strengthening (Blicharski et al., 1988, p.319). Recent research at the David Taylor Research Center has shown that the toughness of ULCB steel with a carbon content of 0.02 - 0.04% was controlled by the inclusion content and grain refinement (Gudas, 1989, p.8).

Bainitic microstructures which form during welding may influence the weld metal strength and toughness. Understanding and controlling the transformation to bainite and its effect on the mechanical properties of the weld metal is essential. Bainite often forms as part of a mixed microstructure containing martensite, Widmanstätten ferrite, pearlite, acicular ferrite or retained austenite. Therefore, it is often difficult to properly identify bainitic microstructures. Bainite forms through a shear transformation from austenite. There are two forms of bainite each distinguished by their lath size and shape along with the size and distribution of carbides. Upper bainite forms at relatively high transformation temperatures. The carbon diffuses in the austenite in front of the growing bainitic ferrite laths forming carbides between the ferrite laths. Lower bainite forms at lower transformation temperatures ($\sim 350°C$). The carbon does not diffuse as quickly

6

and precipitates within the ferrite laths in order to sustain the driving force for the reaction (Pickering, 1978, pp.110-111). Martensite start temperatures for steels containing <0.5% C are above 350°C. Therefore lower bainitic structures do not form in ULCB steels (Samuels, 1980, p.302).

The strength of bainitic structures is dependent upon lath, dislocation, interstitial/substitutional and carbide strengthening. Several studies have associated changes in strength and toughness with the colony (packet) and lath dimensions. Bainitic microstructures contain a higher dislocation density than ferrite formed with a polygonal or Widmanstätten morphology. The dislocation density increases with decreasing transformation temperature and is strongly dependent on the alloying content of the steel as well as the thermomechanical processing. The higher dislocation density strengthens the steel by impeding dislocation movement and thus confining slip. There is experimental evidence which indicates a residual supersaturation of carbon atoms bound to dislocations exists in bainitic ferrite and makes a significant contribution to strength. Carbide strengthening in upper bainite may occur due to the influence of carbides formed at lath boundaries. Such carbides impede the ability of the lath to slip. In lower bainite the carbide dispersion throughout the lath contributes to strengthening described by the Ashby-Orowan relationship. (Edmonds, Cochrane, 1990, pp.1531-1532)

$\sigma_{cem} = An_c \ln(B/n_c)$

n_c = number of effective carbides per unit area (mm^2)

A,B = material constants

Weldability of ULCB steel can be improved by reducing the carbon equivalent value (CEV). Alloying elements such as Ni and Mo are added in large quantities (2-5%) to ultra low carbon steels to depress transformation temperatures into the 500-600 °C range thereby taking advantage of austenite transformation strengthening (Edmonds, Cochrane, 1990, p.1534).

Interlocking acicular ferrite microstructure in weld metals has been widely recognized and accepted to improve toughness. The acicular ferrite microstructure increases the number of times a crack will encounter an interface and thus have to change direction. This increases the toughness of the metal by making it more difficult for the crack to propagate. In a colony of lath martensite all the laths have a similar crystal orientation and a crack may easily propagate through the packet on the cleavage plane. Figure 2 illustrates the crack propagation behavior for three different morphologies clearly indicating the more tortuous crack propagation path associated with acicular ferrite. The goal of much of the research with HSLA and ULCB steels is to maximize the conditions under which acicular ferrite forms (Matlock, Edwards, 1985, pp. 8-9).

Large packets of upper bainite attributed to large alloy additions or low oxygen content have been associated with significant reductions in weld metal toughness. Low oxygen content results in too few weld metal inclusions to nucleate acicular ferrite and thus brittle upper bainite is formed. There is much evidence that the acicular ferrite microstructure is due to primary nucleation on weld metal inclusions along with sympathetic secondary nucleation (Edmonds, Cochrane, 1990, p.1536). Transformation temperatures associated with acicular ferrite are typically below those associated with

upper bainite for steels of similar composition. For this reason and other similarities, Edmonds and Cochrane propose the acicular ferrite microstructure may be a form of bainite. It is important to note carbides do not readily precipitate in ULCB steels because of the low carbon content and thus the true upper bainitic structure may be more appropriately termed bainitic ferrite.

BAINITE   BAINITE & MARTENSITE   ACICULAR FERRITE

(a)   (b)   (c)
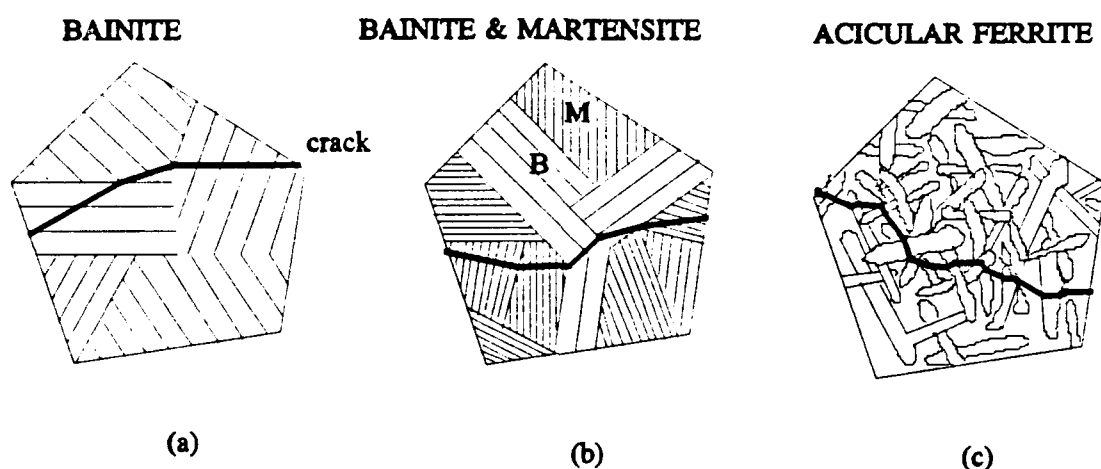
Figure 2
(a) crack deflection at colony boundaries; (b) austenite grains subdivided by bainite; (c) crack deflection at lath boundaries (Edmonds, Cochrane, 1990, p.1533).

Microstructures in ULCB steel weld metal are dependent on the prior austenite grain structure as well as the transformation characteristics of the austenite upon cooling. Classification of the microstructures associated with weld metal is not at all clear cut. Terminology varies depending on the author as many synonyms are used to describe the same microstructure (i.e., proeutectoid ferrite/grain boundary ferrite/polygonal ferrite). At high transformation temperatures grain boundary ferrite forms on prior austenite grain

9

boundaries and at slightly lower temperatures proeutectoid ferrite forms as sideplate ferrite. The ferrite usually grows into the grain on one side. Widmanstätten ferrite forms as the transformation temperature is lowered. The ferrite sideplates associated with Widmanstätten ferrite grow long and needlelike into the grain. At reduced transformation temperatures acicular ferrite forms. Most acicular ferrite exists within grains of prior austenite and have large angles between adjacent laths. Bainite and martensite are produced respectively as the transformation temperature is further reduced. The cooling rate significantly influences the solidification microstructure. The cooling time from 800 to 500°C is widely accepted as the basis for the thermal conditions under which the austenite to ferrite transformation occurs. For welding of thick plates Grong and Matlock propose a simple correlation to determine the time to cool from 800 to 500°C:

$$\Delta t_{800 \to 500°C} \approx 5\eta E$$

η = arc efficiency

E = heat input (MJ/m)

Typically, rapid cooling times (<5s) are associated with martensitic and/or bainitic microstructures whereas moderate cooling times (5-100s) promote acicular ferrite, ferrite sideplates and/or grain boundary ferrite. For long cooling times (>100s) polygonal ferrite and/or pearlite dominate (Grong, Matlock, 1986, p.37). Figure 3 indicates the effects of two different cooling rates on weld metal microstructural transformations. The chemical composition of ULCB steel controls the bainite start temperature and the bainite

start temperature has an inverse linear relationship with the strength of bainitic steels (See Figure 4) (Blicharski et al., 1988, p.326).

The strength and toughness of ULCB steel weldments are influenced by a multitude of factors. The alloy content, welding process, weld pool geometry, heat input rate, cooling rate and presence of nonmetallic inclusions all influence the final microstructure. The goal of welding research is to identify the proper combination of all these factors to optimize weld metal strength and toughness.
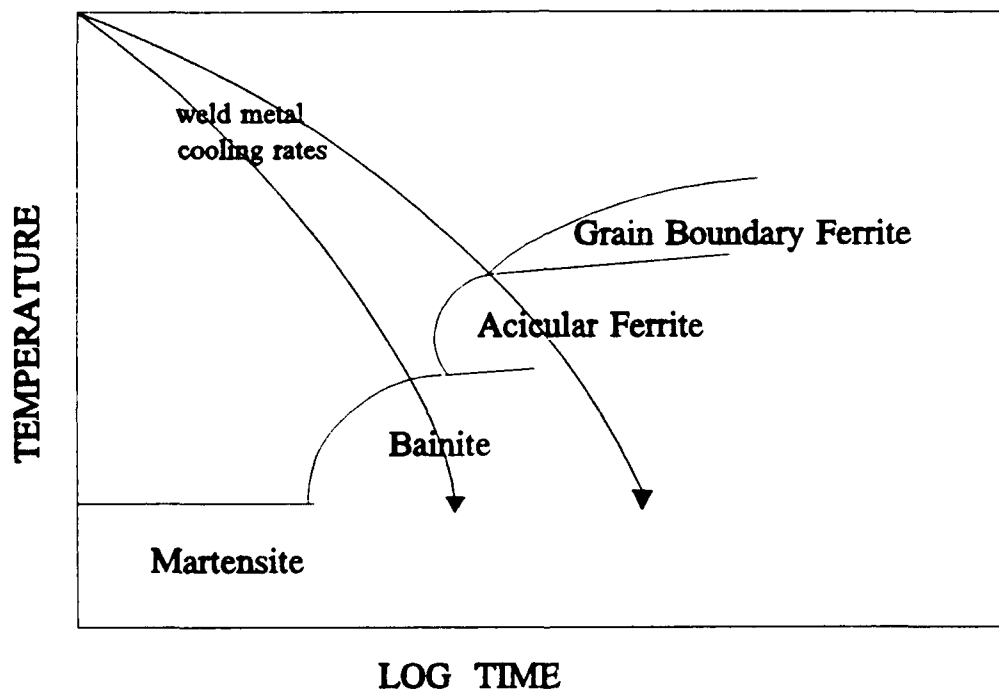
Figure 3

Continuous cooling transformation curves illustrating the effects of varying weld metal cooling rates on the microstructural development.

12
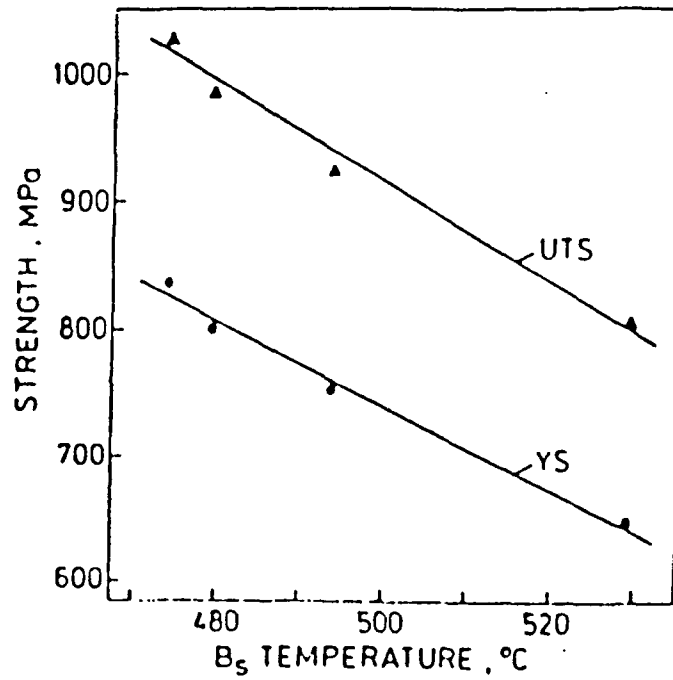
Figure 4

Relationship between bainite start temperature and strength (Blicharski et al., 1988, p.324).

C. WELDING METHODS UTILIZED IN ANALYSIS

1. Tungsten Inert Gas (TIG)

Tungsten inert gas welding, also known as gas tungsten arc welding (GTAW), produces a weld through the development of an arc between a non-consumable tungsten electrode and the base metal (See Figure 5). TIG welding is the cleanest arc welding process due to the use of inert shielding gases and a short, stable arc. Inert gases (Ar, He) shield the electrode and weld zone to protect the molten weld metal from oxidation or contamination from the surrounding atmosphere. Argon is preferred over helium in TIG welding since it is easier to ionize (ease of arc initiation), has a smaller voltage drop across the arc and is heavier than helium thus providing a better shielding effect (Kou, 1987, p.11).

The contact tube conducts current from the power source to the non-consumable electrode. Two types of electrical setups are utilized in TIG welding. In direct-current straight polarity (DCSP) the electrode is connected to the negative terminal of the power source. This yields a strong heating effect on the base metal producing narrow, deep welds. Such welds are normally preferred. The other method, direct current reverse polarity (DCRP), generates the heating effect at the tungsten electrode. This requires large diameter, water-cooled electrodes and produces undesirable shallow welds (Kou, 1987, p.10).
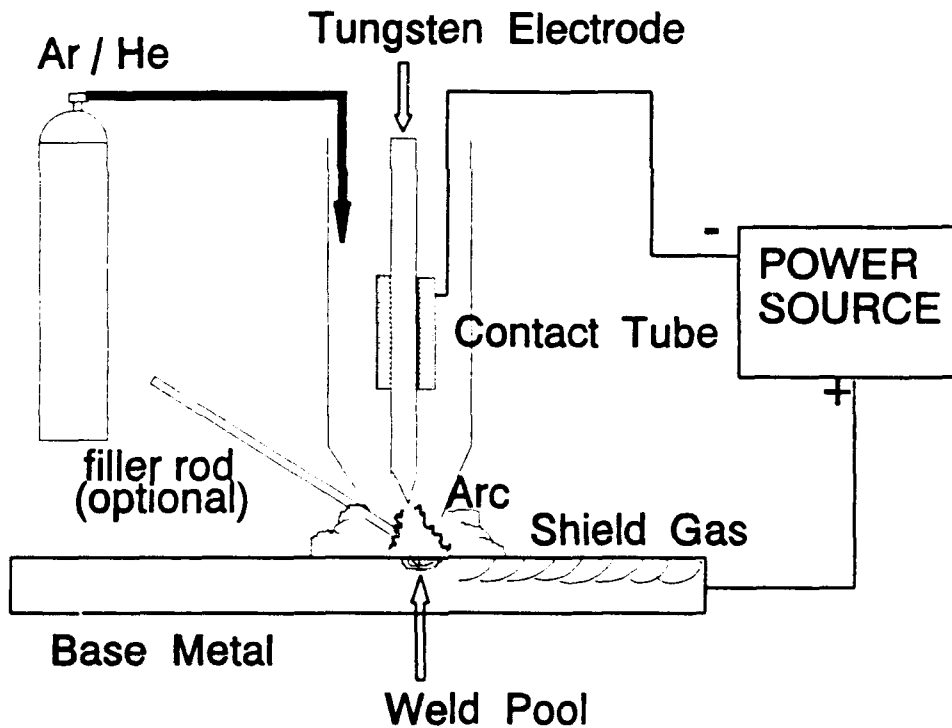
Figure 5
Tungsten Inert Gas (TIG) welding process.

2. **Metal Inert Gas (MIG)**

Metal inert gas (MIG), also known as gas metal arc welding (GMAW), produces a weld by heating metals with an arc established between a consumable electrode (continuously fed) and the base metal (See Figure 6). A shielding gas protects the weld metal but the MIG welding process is not as clean as the TIG process. The consumable electrode produces a less stable arc and the larger arc lengths associated with MIG welding may adversely affect the performance of the shielding gases.

Direct current reverse polarity (DCRP) is used in MIG welding to produce a stable arc, smooth metal transfer and sufficient weld penetration. There are three basic

15

modes of metal transfer in MIG welding. First, short circuiting, in which the filler metal
is transferred to the weld pool when the consumable electrode is in contact with the weld
pool. Secondly, globular metal transfer, in which the metal drops fall to the weld pool
under the force of gravity. The final mode, spray, attracts the metal drops to the weld
pool under the influence of electromagnetic forces.
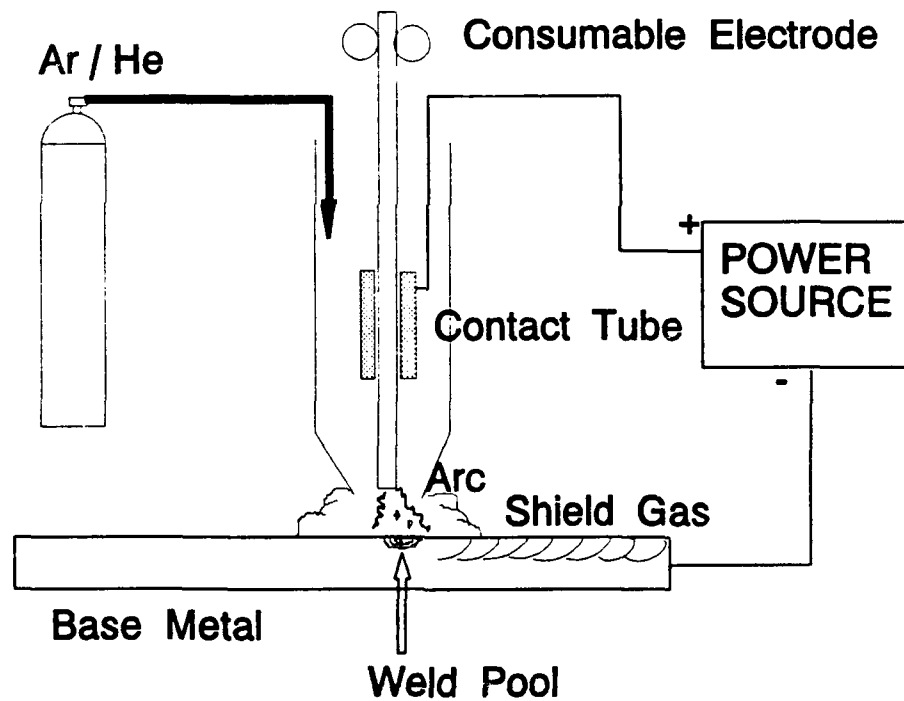
Figure 6
Metal Inert Gas (MIG) welding process.

D. INFLUENCE OF ALLOYING ELEMENTS ON WELD METAL STRENGTH AND TOUGHNESS

Alloying elements are introduced into the weld metal through dilution from the base metal, directly from the filler wire and from the welding flux. The majority of the alloying elements (C, Ni, Cr, Mo, Mn) increase hardenability. However, the influence of each individual alloying element is often difficult to discern due to the numerous interacting factors involved in the microstructural development. The balanced addition of alloying elements is essential to control the weld metal microstructure to achieve the desired strength and toughness.

1. Carbon

Carbon is a solid solution strengthener and greatly improves hardness. Increasing the carbon content results in grain size refinement and elevated levels of carbides. The strengthening effect of carbon is principally due to the formation of carbides (Abson, Pargeter, 1986, p.148). Carbides strengthen but may also serve as crack nucleation sites. Carbon content is kept low to avoid hydrogen assisted cold cracking and brittle fracture initiation in the weld region (Grong, Matlock, 1986, p.38). There have been conflicting reports on the effect of low level carbon content on weld metal toughness. Several studies indicate Charpy toughness decreases as carbon content increases from 0.1% to 0.2% in gas shielded weld deposits (Abson, Pargeter, 1986, p.153). Therefore it is desirable to maintain carbon levels below 0.10%. Figure 7 shows the relative hardness effect of several steel alloying elements.

17
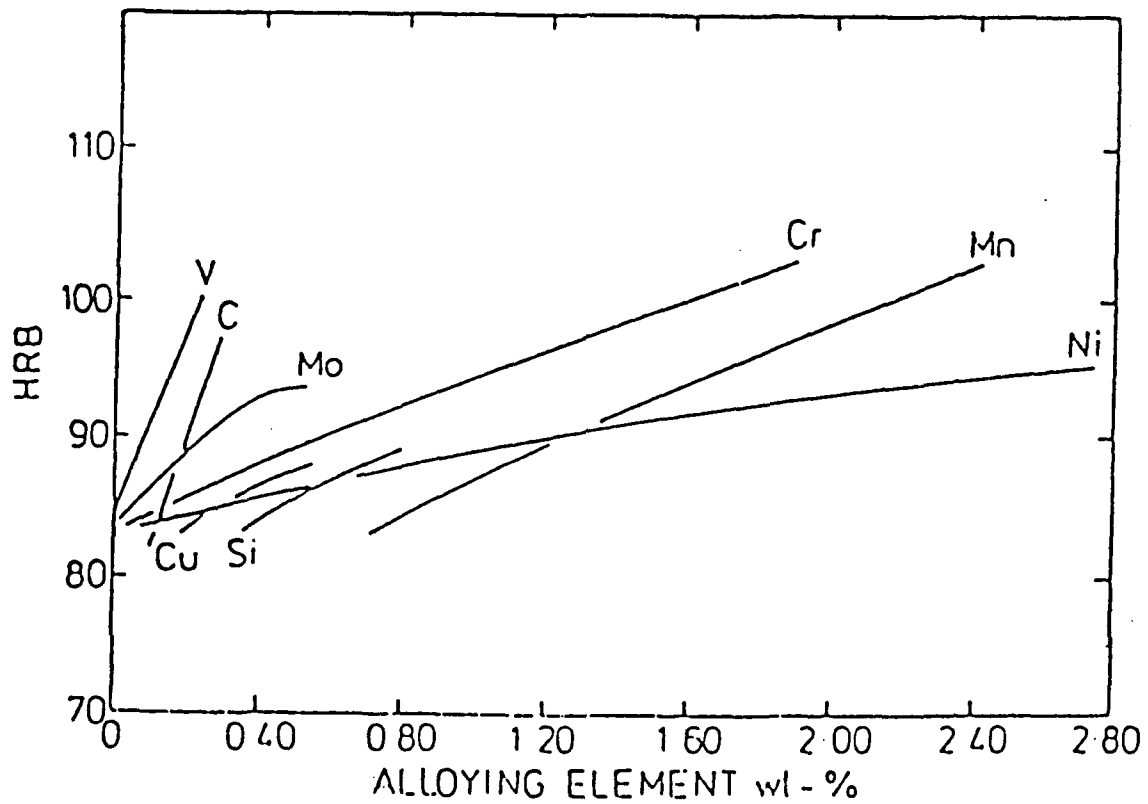
Figure 7
Relative effect of alloy additions on hardness (Abson, Pargeter, 1986, p.145).

2. Manganese

Manganese serves as a weak deoxidizer and has a solid solution strengthening effect in weld metals. Manganese increases the amount of acicular ferrite at the expense of grain boundary ferrite (Abson, Pargeter, 1986, p.145). The precipitation of MnS

instead of FeS reduces the tendency for crack formation in the grain boundaries associated with the low melting point FeS phase (Kiessling, Lange, 1978, pp.96-97). Several studies indicated Charpy toughness increased with increasing manganese content with optimum levels ranging from 1 to 1.5 percent. The improved toughness is largely attributed to refinement of the microstructure (Abson, Pargeter, 1986, pp.154-159). Manganese lowers the transformation temperature of austenite to ferrite and acts as an austenite stabilizer.

3. Molybdenum

Molybdenum is used primarily to improve strength but can also improve toughness and increase the amount of acicular ferrite present (Abson, Pargeter, 1986, p.166). The role of molybdenum and chromium is not fully understood but the formation of molybdenum or chromium carbides may restrict the formation of proeutectoid ferrite at the prior austenite grain boundaries either by pinning or dragging effects (Grong, Matlock, 1986, p.38).

4. Chromium

Chromium is a strong carbide former and serves as a solid solution strengthener. In quenched and tempered steels chromium acts as a hardenability agent (Hertzberg, 1989, p.376).

5. Silicon

Silicon is used in combination with manganese as a deoxidizing agent. High levels of silicon (>0.5%) are generally detrimental to weld metal toughness (Abson, Pargeter, 1986, p.159).

6. Nickel

Nickel lowers the austenite to ferrite transformation temperature and refines the acicular ferrite thereby improving toughness. Nickel also serves as an austenite stabilizer (Abson, Pargeter, 1986, p.170).

7. Titanium

Titanium precipitates of carbides or nitrides may serve as nucleation sites for acicular ferrite. Titanium containing inclusions have been identified as being particularly effective in the nucleation of intragranular acicular ferrite (Kiessling, 1989, p.105).

8. Aluminum

Aluminum is an extremely effective deoxidizing agent and refines the grain structure of weld metal through the formation of aluminum nitrides which pin grain boundaries and inhibit grain growth (Hertzberg, 1989, p.376).

E. NONMETALLIC INCLUSIONS IN STEEL WELDMENTS

Inclusions play an important role in controlling the properties of steel weldments and weld metal. Depending on their size, composition and distribution, inclusions may have an adverse or beneficial influence on weld metal properties. Adversely, inclusions may serve as both ductile and brittle fracture initiation sites. Small inclusions ($<2\mu$m) may be used to control the microstructure of the weld metal and base metal by restricting grain growth and aiding in the nucleation of desirable acicular ferrite (Kiessling, 1989, p.102).

1. Sources of Nonmetallic Inclusions

Inclusions commonly found in weldments are either indigenous or exogenous. Indigenous inclusions originate from deoxidation reactions (oxides) or solid state precipitation reactions (nitrides, carbides) occurring in the molten or solidifying steel bath. Indigenous inclusions are typically oxides or sulfides and may be formed either by additions to the steel or due to changes in solubility during the solidification process. Exogenous inclusions are formed through the entrapment of electrode slag, refractories, electrode coatings or other material with which the molten steel comes into contact. They are characteristically large, sporadic in occurrence, irregular in shape and complex. Exogenous inclusions are always detrimental and should be avoided.

2. Inclusion Size, Quantity and Distribution

The volume fraction and total number of nonmetallic inclusions in steel weld metal is much higher (typically 10^7 -10^9 particles per mm^3) than that of normal cast steel.

The limited time for growth and separation during the deoxidation process results in small ($< 1\mu$m) finely dispersed inclusions. The particle size and distribution is a function of the welding atmosphere, welding method, flux, consumables and subsequent cooling rate. Variations in the heat input also strongly influence the inclusion size distribution. (Grong, Matlock, 1986, pp.32-33)

Small inclusions (< 1-2μm) influence the properties of the weld metal by affecting the microstructure and thus toughness. It is important to control the microstructural transformation products in order to produce a beneficial vice detrimental effect.

Large inclusions (> 1-2μm) increase the risk of cracking and reduce weld metal toughness and fatigue strength.

3. Deoxidation of Steel Weld Metals

Deoxidation of molten steel weld metal improves toughness (Kou, 1987, pp.70-82). Elements with a high affinity for oxygen serve as deoxidizing agents in the manufacturing of steel. Deoxidizing elements such as aluminum, silicon and titanium reduce the amount of oxygen in the steel since they have a free energy of oxide formation lower than that of FeO. Typical curves indicating the relative concentration of oxygen and deoxidizing elements for those relevant to steelmaking are shown in Figure 8. Elements represented by curves shown below the typical weld metal oxygen content (shaded region) are associated with nonmetallic inclusions.

There are three major steps in steel deoxidation - nonmetallic inclusion nucleation, growth and phase separation. Figure 9 illustrates the average particle size

22

with reaction time. In welding, this reaction is usually not carried to completion resulting in a higher concentration and larger inclusions in the weld metal (Ramsay, Matlock, Olson, 1988, p.10).

Buoyancy plays an insignificant role in the separation process of oxide inclusions from the weld pool. Increased weld pool retention time provides for enhanced particle growth and flotation resulting in more efficient deoxidation. The average velocity, v, of the ascending particles relative to the liquid is approximated by Stoke's Law (Grong et al., 1986, p.1798):

$$v = (gd^2 \Delta \rho)/(18\eta)$$

where g is a gravitational constant, d is the particle diameter, $\Delta \rho$ is the density difference between liquid steel and inclusions, and η is the steel viscosity. The Stokes' parameter, $g\Delta\rho/18\eta$, for manganese-silicates is $0.6(\mu msec)^{-1}$. Assuming an average nonmetallic inclusion diameter of $0.5\mu m$ this yields a flotation velocity of $0.15\mu m/s$. Such a velocity is several orders of magnitude below the average fluid flow velocity in the weld pool indicating the buoyancy effect alone is insignificant in promoting the flotation of nonmetallic inclusions out of the weld pool before solidification. (Grong et al., 1986, p.1803)
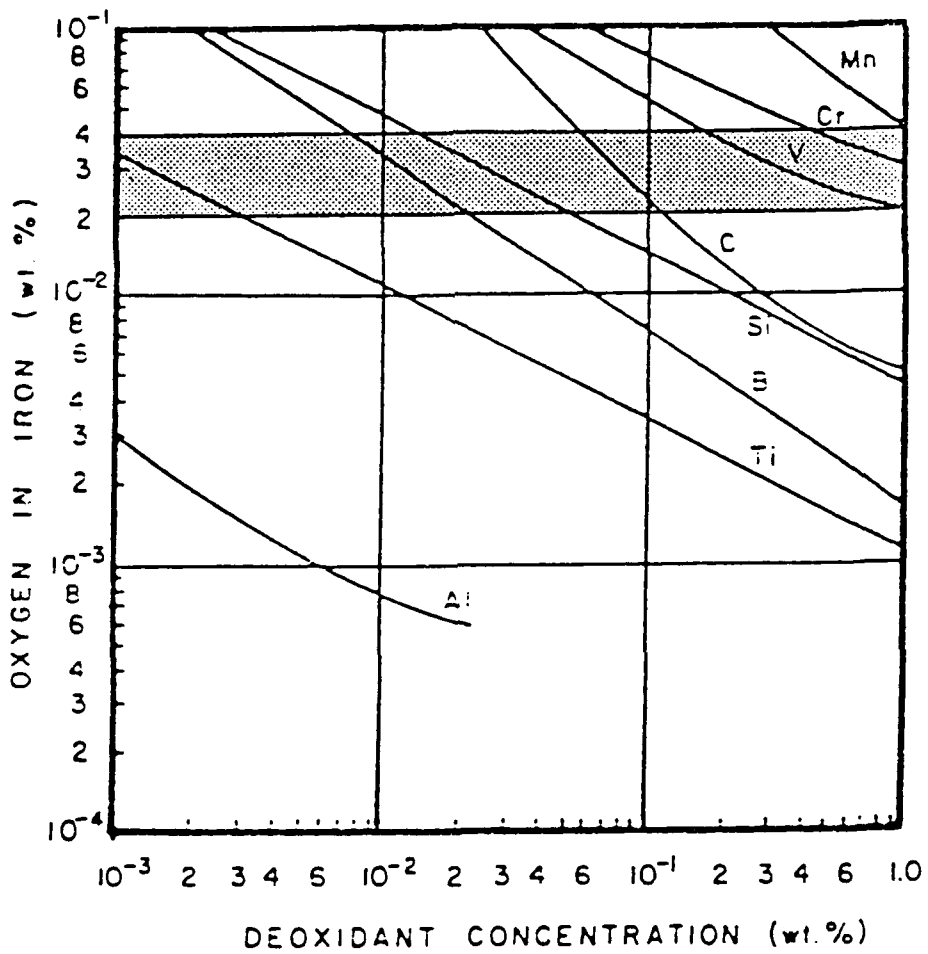
Figure 8
Relative deoxidizing strength of typical alloying elements (Ramsay et al., 1988, p.8).

24

AVERAGE PARTICLE SIZE

Nucleation Stage
• Homogenoous nucleation
• Heterogenoous nucleation

Growth Stage
• Diffusion of reactants in the melt to the oxide nuclei
• Particle coalescence

REACTION TIME

Separation Stage
• Buoyancy
• Surface tension
• Stirring
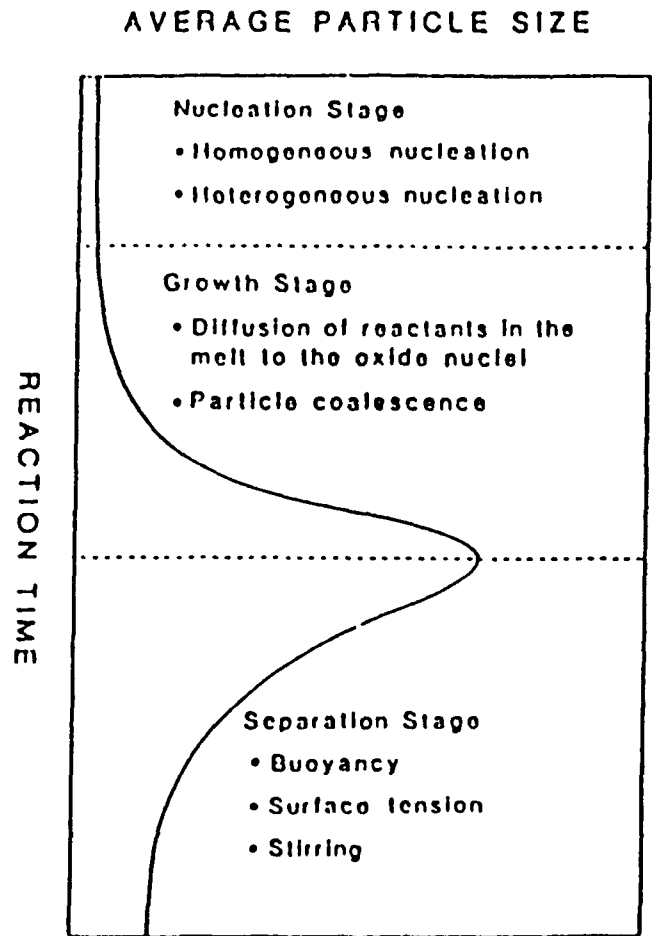
Figure 9
Three major steps in steel deoxidation (Grong et al., 1986, p.1798).

Grong and Christensen developed and Grong, et al., later substantiated a sequence of deoxidation reactions based on a "hot" and "cold" part of the weld pool (See Figure 10). The "hot" region of the weld pool is characterized by simultaneous oxidation and deoxidation of the metal. The turbulent nature of the weld pool in this region serves to stimulate particle growth and phase separation. The precipitated slag particles are forced to the surface due to the highly turbulent conditions. The "cold" region of the weld pool is characterized by poor mixing in the melt resulting in the precipitated slag particles becoming trapped in the solidifying weld pool. The less turbulent conditions in the "cold" region favor nucleation over growth and most of the precipitated slag particles are trapped in the form of finely dispersed inclusions (Grong et al., 1986, p.1799). Grong, et al., also concluded the weld metal oxygen content can be reduced by increasing the weld metal manganese-to-silicon ratio. An interesting aspect of Grong's work was the high manganese-to-silicon ratio weld metal contained a higher concentration of smaller trapped inclusions (Grong et al., 1986, p.1802).
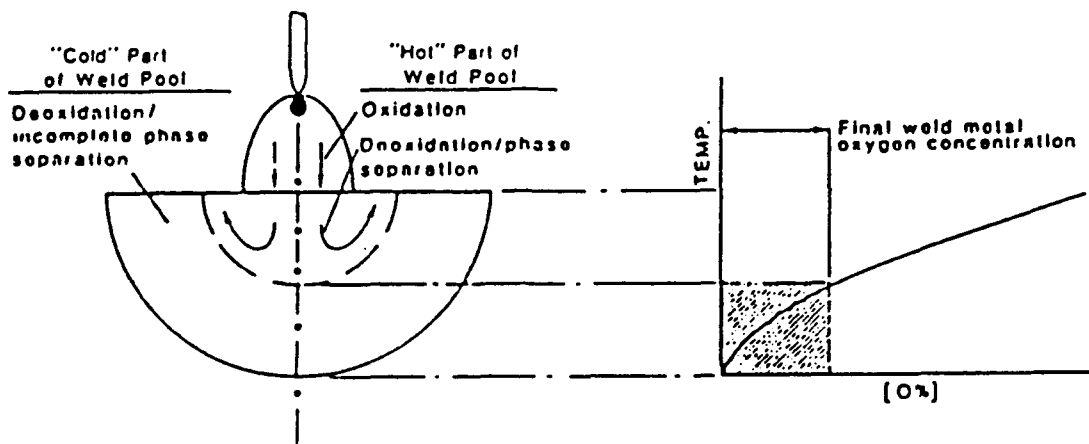
Figure 10
Weld pool deoxidation reactions based on hot and cold parts of the weld pool (Grong et al., 1986, p.1799).

27

4. Influence on Prior Austenite Grain Size

A well refined prior austenite grain size improves weld metal toughness. Small grain size provides increased grain boundary area for the nucleation of grain boundary ferrite. Prior austenite grain size is dependent on the oxide inclusion content in the weld metal. Small inclusions are more effective at pinning grain boundaries and hindering grain growth. The Zener relationships determine the limiting grain size, D_L, and the drag force, F_d, an inclusion exerts on a migrating boundary.

$$D_L = 2d/3f \qquad\qquad F_d = d\gamma\cos\theta\sin\theta$$

d = average inclusion diameter γ = specific interfacial energy

f = volume fraction of inclusions θ = angle inclusion meets grain boundary
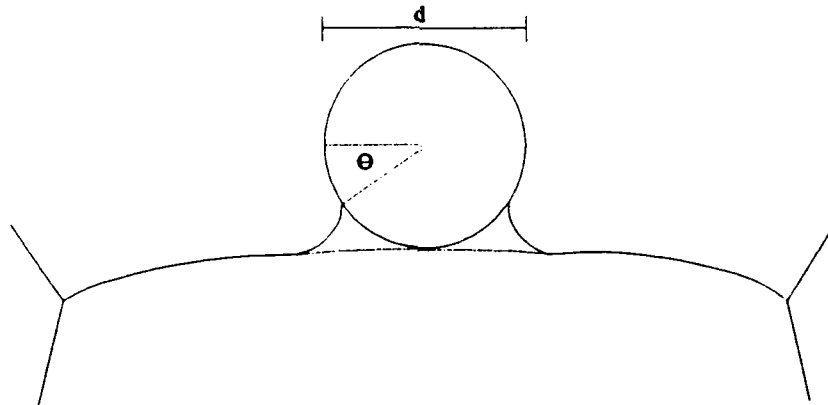
Figure 11
Inclusion/grain boundary relationship for Zener correlation (Ramsay et al., 1988, p.17).

28

Inclusions greater than the critical diameter are not effective at pinning austenite grain boundaries. The austenite grain size decreases with increasing numbers of sufficiently small inclusions. The prior austenite grain size also decreases with increasing weld metal oxygen content reflecting the corresponding increase in the total number of grain boundary pinning oxide inclusions in the weld metal. (Ramsay, Matlock, Olson, 1988, pp.15-17)

5. Nucleation of Acicular Ferrite

All studies dealing with the nucleation of acicular ferrite (AF) agree this finely grained microstructure consisting largely of intragranularly nucleated Widmanstätten ferrite improves weld metal toughness. Thus, the role nonmetallic inclusions play in the nucleation of acicular ferrite is of vital importance. Abson et al., studied the effects of changes in weld metal oxygen and sulfur levels (hence total inclusion volume fraction) on the nucleation of acicular ferrite. The results indicated a particular range of oxygen content which favored the nucleation of acicular ferrite. Below this optimum oxygen content (0.030%) the structure was mainly bainitic with little or no acicular ferrite. Thus, the proper oxygen content is important since too low an oxygen content will yield too few nucleants and choke the formation of acicular ferrite while too high an oxygen content results in ineffective nucleants. The inclusion type and size was deemed more important than the total inclusion volume fraction in influencing the nucleation of acicular ferrite (Abson et al., 1978, p.75). Intragranular nucleation of acicular ferrite at inclusions is preferentially associated with Al-Mn silicates which are not covered with a sulfide coating and contain a small amount of Ti (Kiessling, 1989, p.105).

29

Inclusions promote the intragranular nucleation of ferrite in three ways (Ricks, Howell, Barritte, 1982, pp.735-736):

1. They reduce the energy barrier to nucleation by acting as an inert substrate.

2. The nucleated ferrite orients itself with respect to the inclusion and the austenite such that low-energy interfaces form between the austenite and the inclusion.

3. The inclusions affect the local chemistry of the austenite increasing the transformation driving force.

The inclusion size distribution influences whether the inclusions will be associated with the grain boundaries or located intragranularly. High acicular ferrite weld metals are associated with large austenite grains and large ($>0.2\mu$m) inclusions. Whereas, high oxygen content weld metals with large amounts of grain boundary ferrite are associated with fine austenite grain size and small ($<0.1\mu$m) inclusions. The weld metal cooling time must be of sufficient duration (>5s) to favor the nucleation of acicular ferrite (Grong, Matlock, 1986, p.37). Overall, the nucleation of acicular ferrite is optimized with large austenite grains, a high density of intragranular inclusions and sufficient weld metal cooling time. (Kiessling, 1989, pp.106-107)

F.   SCOPE OF THE PRESENT WORK

Although extensive research has been conducted to develop an easily weldable high strength weld metal with maximum strength and toughness there remain many unanswered questions. This study focused on ULCB steel weldments with both ULCB and HY-130 base metals. The major issues investigated were the effect of varying weld

metal heat input, the influence of HY-130 and ULCB parent metals and the effect of a reactive cover gas. All of these factors influence the formation of nonmetallic inclusions in the weld metal. Nonmetallic inclusions were identified with respect to size, distribution and composition and the effect (if any) on microstructural development was investigated. The heat input rate and subsequent cooling rate determined the microstructural as well as macrostructural development. An important aspect of this study investigated the influence of the heat input rate on the degree of constitutional supercooling and thus macrostructural development. ULCB steel weldments were evaluated at 1.4MJ/m and 2.8MJ/m. The effect of ULCB and HY-130 parent metals was studied largely from the influence on the mechanical properties and the carbon content of the ULCB weld metal. The introduction of reactive cover gases had profound effects on the inclusion density and the formation of carbides both of which impacted the mechanical properties. The study of ultra low carbon steel weldments continues to be a fascinating area of research in which much has been done and yet there is still much to be accomplished.

III. PROCEDURAL OVERVIEW

A. WELDMENT SAMPLES

Ultra Low Carbon Bainitic (ULCB) steel weldment samples were supplied by David W. Taylor Naval Research Center in the form of charpy and tensile test specimens. The ULCB steel was Vacuum Induction Melted at the U.S. Steel Research Center in Monroeville, Pennsylvania and then Vacuum Arc Remelted at the Oregon Graduate Institute in Beaverton, Oregon. Next the steel was cast into an ingot 18 inches in length and 9 inches in diameter. Plates of 1.25 inch thickness were sliced out of the center of the ingot. The ULCB steel filler wire was also cut from the same ingot casting as the base metal. The HY-130 base steel was hot worked, quenched and tempered. Table I provides the elemental breakdown of the specimens studied along with the welding process, cover gas and heat input rate. Charpy specimens were cut transverse to the weld beads (See Figure 12). The tensile test specimens were taken axially from the weld bead. The nondeformed section was cut, mounted in bakelite and polished for suitable SEM observation.
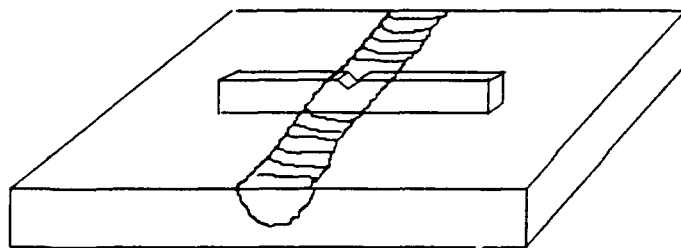
Figure 12
Dimensions and orientation of Charpy weldment samples.

TABLE I

WIRE MATERIAL (WELD METAL)	ULCB STEEL	ULCB STEEL	ULCB STEEL	ULCB STEEL
BASE METAL	N/A	HY-130 STEEL	ULCB STEEL	HY-130 STEEL
WELDING PROCESS	N/A	TIG	TIG	MIG
HEAT INPUT RATE	N/A	1.4 MJ/m	1.4 MJ/m 2.8 MJ/m	1.4 MJ/m
SHIELDING GAS	N/A	Ar-He	Ar-He	M-5 (5% CO_2)
CARBON	0.036%	0.027%	0.016%	0.038%
MANGANESE	2.300%	1.680%	2.170%	1.740%
CHROMIUM	0.480%	0.500%	0.490%	0.490%
NICKEL	5.090%	5.130%	5.140%	5.030%
MOLYBDENUM	2.800%	2.100%	2.760%	2.360%
COPPER	0.006%	0.012%	0.006%	0.010%
SULFUR	0.005%	0.005%	0.003%	0.005%
SILICON	0.190%	0.190%	0.180%	0.160%
NITROGEN	0.004%	0.025%	0.009%	0.011%
NIOBIUM	0.087%	0.068%	0.091%	0.074%
TITANIUM	0.019%	0.017%	0.018%	0.016%
ALUMINUM	0.041%	0.019%	0.024%	0.026%

Specimen data.

B.   EXPERIMENTAL PROCEDURE

The samples were finely polished using a series of progressively finer emery papers. The final polishing was conducted on polishing wheels using 6 μm and then 1μm diamond paste. The initial inclusion study performed on the ULCB steel weldments was accomplished using the Cambridge Stereo Scan S200 SEM in conjunction with the Kevex 8000 Energy Dispersive X-ray analysis spectrometer. The SEM was operated using a LaB$_6$ filament. The accelerating voltage was 20 KV and the specimen working distance was 18mm. The data collection for each TIG weldment containing ULCB filler metal consisted of evaluating forty fields running from the bottom to the top of the weld metal and one hundred random fields associated with the base metal. The MIG weld sample was evaluated by looking at three fields in the weld metal (bottom, middle, top) and fifty random fields associated with the base metal. This was necessitated due to the large increase in the number of inclusions observed in this sample. Each field was viewed at 2,000x magnification. For each inclusion the diameter and shape was recorded and EDX analysis was performed. A comparative test was performed clearly showing a more accurate representation of the matrix and inclusion elemental make-up was achieved using the RASTER to "frame" the inclusion. Thus, the RASTER method was used vice putting the spot on the inclusion. A background EDX spectrum for the base metal and weld metal was obtained for later use in the matrix stripping routine.

Next the samples were etched using 2% nital solution. The microstructure was observed using optical microscopy and the scanning electron microscope. Carbon

extraction replicas suitable for TEM observation were produced in accordance with Appendix C. The carbon extraction replicas greatly assisted in the accurate determination of the inclusion elemental make-up.

IV. RESULTS AND DISCUSSION

A. MECHANICAL PROPERTIES

The mechanical properties of the ULCB steel weldments were shown to be largely dependent on the heat input and to a lesser extent the base plate composition, cover gas and nonmetallic inclusion make-up. The mechanical properties are presented in Table II and Charpy data in Figure 13. A significant improvement in the ULCB weld metal properties was achieved with the higher (2.8MJ/m) heat input. In doubling the heat input the yield strength increased from 869MPa (126ksi) to 931MPa (135ksi) and the fracture appearance transition temperature (FATT) decreased from 35°C at 1.4MJ/m to -4°C at 2.8MJ/m heat input. The upper shelf energy increased from 81^+J at 1.4MJ/m to 129J at 2.8MJ/m heat input. The toughness of the two ULCB steel weldments utilizing the HY-130 base plates was poor. This was attributed to carbon pickup from the HY-130 base metal occurring in the fusion zone. The ULCB/HY-130 MIG weldment had the poorest mechanical properties. In addition to carbon pickup from the HY-130 base metal the M-5 cover gas markedly increased the inclusion density as well as promoting the formation of carbides.

TABLE II

SAMPLE	ULCB/ULCB TIG 1.4MJ/m	ULCB/ULCB TIG 2.8MJ/m	ULCB/HY130 TIG 1.4MJ/m	ULCB/HY130 MIG 1.4MJ/m
YS MPa(ksi)	869 (126)	931 (135)	862 (125)	931 (135)
UTS MPa(ksi)	1000 (145)	1020 (148)	1082 (157)	1020 (148)
FATT °C(°F)	35 (95)	-4 (25)	>49 (>120)	29 (85)
USE J(ft-lbf)	>81 (>60)	129 (95)	>56 (>41)	52 (38)
%Elongation	17	19	15	1
%Reduction Area	65	66	53	6

Mechanical properties.

CVN Energy for ULCB Weld Metal
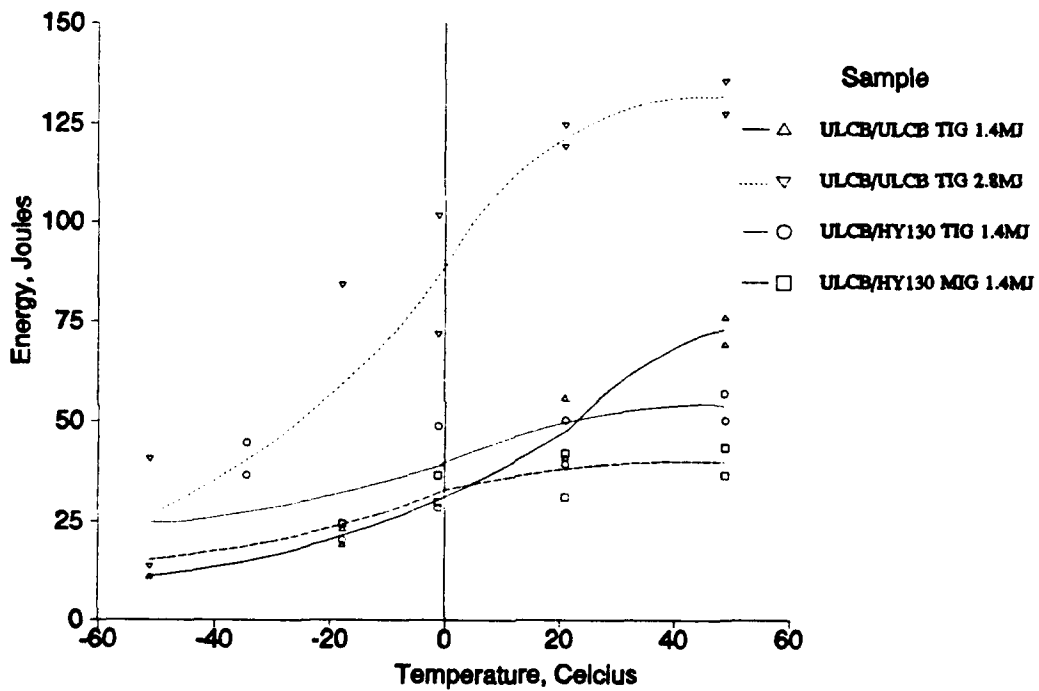
Figure 13

Charpy specimen data provided by David Taylor Naval Ship Research and Development Center.

B. MACROSTRUCTURAL ANALYSIS

The resulting macrostructures of the four experimental welds are presented in Figures 14 and 15. The higher heat input for the ULCB/ULCB steel weldment clearly formed a tough, finely grained macrostructure while the lower heat input generated columnar and dendritic growth. Initial weld pool solidification begins at the fusion boundary where the partly melted base metal grains serve as nucleation sites for columnar growth. Grain growth occurs normal to the fusion line in the direction of the maximum temperature gradient (G) in the weld pool. The lower heat input develops a more rapid cooling rate and thus a larger temperature gradient. A lower degree of constitutional supercooling accompanies this larger temperature gradient resulting in large columnar/dendritic growth structures. Figure 16 illustrates constitutional supercooling in alloy solidification and the relationship between the temperature gradient and the degree of constitutional supercooling. Dendritic growth continues until the subcooled liquid adjacent to the solidification front reaches the equilibrium temperature. The higher heat input develops a slower cooling rate and a reduced temperature gradient in the weld pool. A fully equiaxed grain structure was achieved with the higher heat input due to the large region of constitutional supercooling resulting from the less severe temperature gradient. A large region of constitutional supercooling enhances equiaxed grain growth by forming solid nuclei in front of the solid-liquid interface. Figure 17 illustrates the weld metal solidification structures as a function of the degree of supercooling.
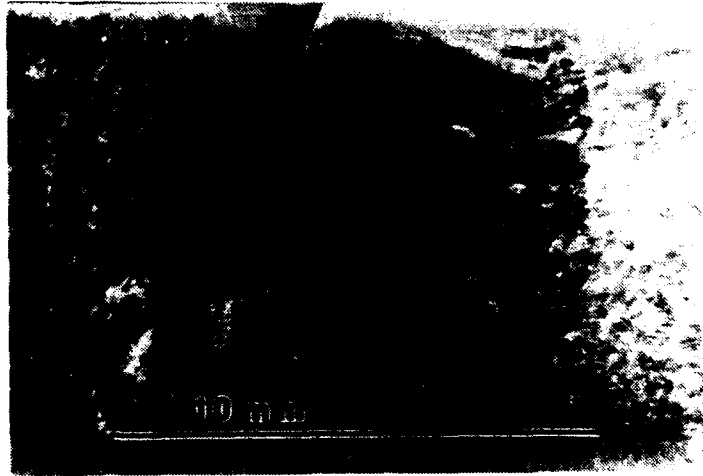
(a)
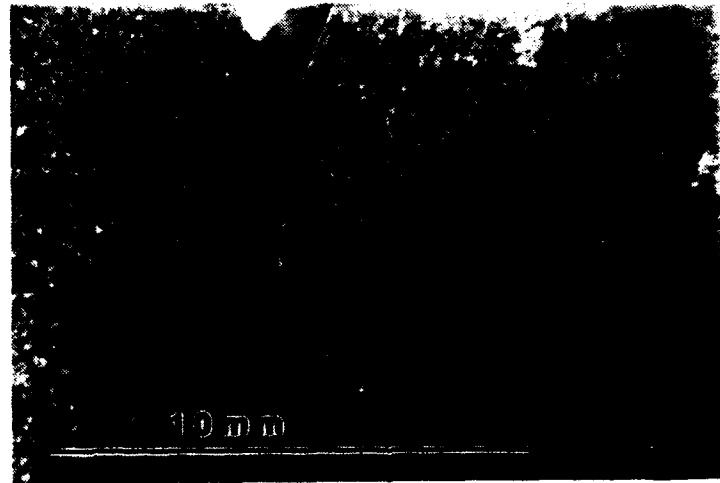
(b)
Figure 14
Macrostructures for (a) ULCB base and weld metal; TIG; 1.4MJ/m and (b) ULCB base
and weld metal; TIG; 2.8MJ/m.
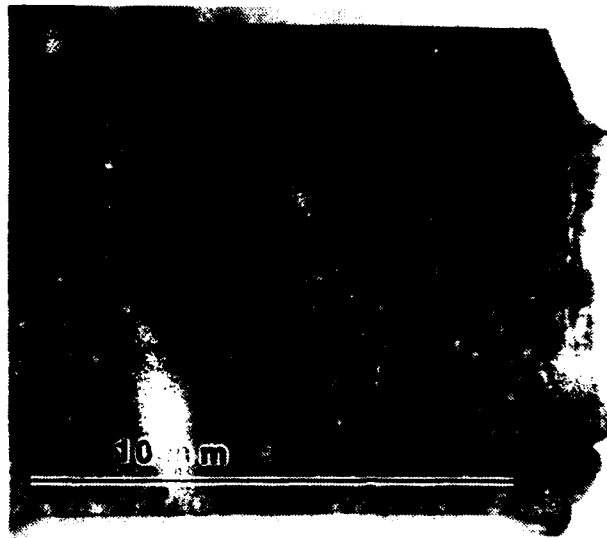
(a)
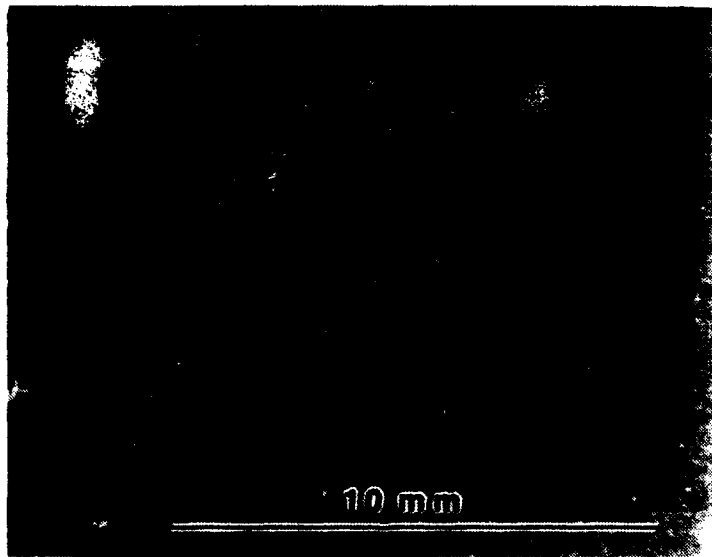
(b)

Figure 15

Macrostructures for (a) HY-130 base and ULCB weld metal; TIG; 1.4MJ/m and
(b) HY-130 base and ULCB weld metal; MIG with M-5 cover gas; 1.4MJ/m.
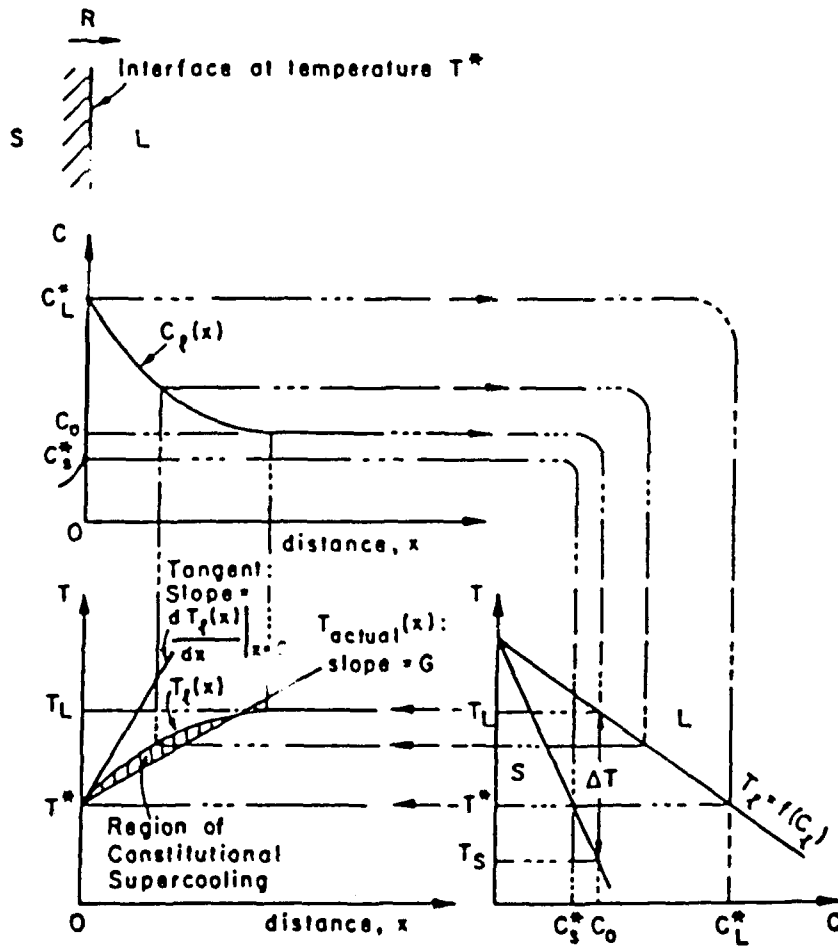
Figure 16

Constitutional supercooling in alloy solidification (Kou, 1987, p.133).
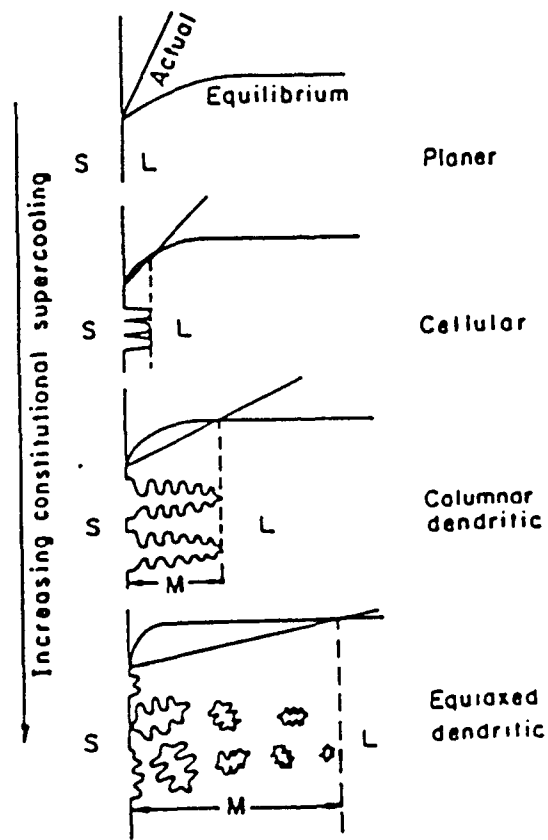
Figure 17

Weld metal solidification structure as a function of the degree of supercooling (Kou, 1987, p.135).

44

C. MICROSTRUCTURAL ANALYSIS

The resulting microstructures of the four experimental weldments were evaluated using optical, scanning electron and transmission electron microscopy. The major factor determining the microstructure of the as-deposited weld bead was the heat input rate. The heat input rate determines the cooling rate and thus the austenite transformation products. The cooling times for the heat input rates studied were calculated using nominal arc efficiency values of 0.4 and 0.75 for TIG and MIG weldments respectively. However, the arc efficiency values actually span a fairly wide range and the cooling time is influenced when welding is performed on base plates of different material due to variations in the steel thermal conductivity (Grong, Matlock, 1986, p.37).

TIG 1.4MJ/m:

$$\Delta t_{800\rightarrow500^\circ C} \approx 5\eta E = 5(0.4)(1.4) = 2.8s$$

TIG 2.8MJ/m:

$$\Delta t_{800\rightarrow500^\circ C} \approx 5\eta E = 5(0.4)(2.8) = 5.6s$$

MIG 1.4MJ/m:

$$\Delta t_{800\rightarrow500^\circ C} \approx 5\eta E = 5(0.75)(1.4) = 5.3s$$

The lower heat input results in a shorter cooling time promoting the formation of martensitic and/or bainitic microstructures. The longer cooling time associated with the higher heat input shifts the cooling curve to the right away from the martensite and bainite regions and towards the acicular ferrite region. There was some evidence of inclusion nucleated ferrite laths. However, this nucleation mechanism was not dominant

45

as the maximum cooling time calculated ($\sim 5s$) still favored the formation of bainitic microstructures. Figures 18 and 19 illustrate the effect of nonmetallic inclusions on the weld metal microstructure.
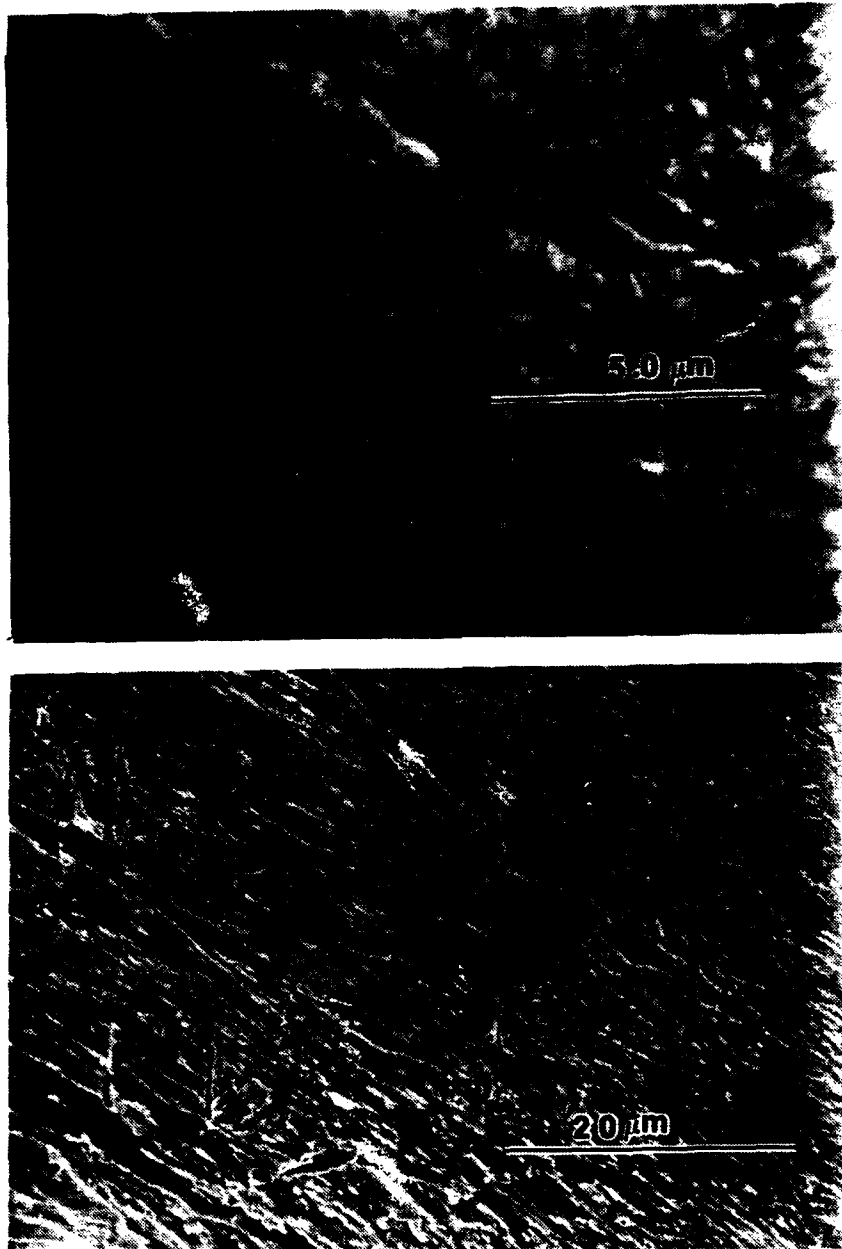

Figure 18
Top - carbon extraction replica, magnification 7,200x; Bottom - SEM micrograph, magnification 2,000x.

46
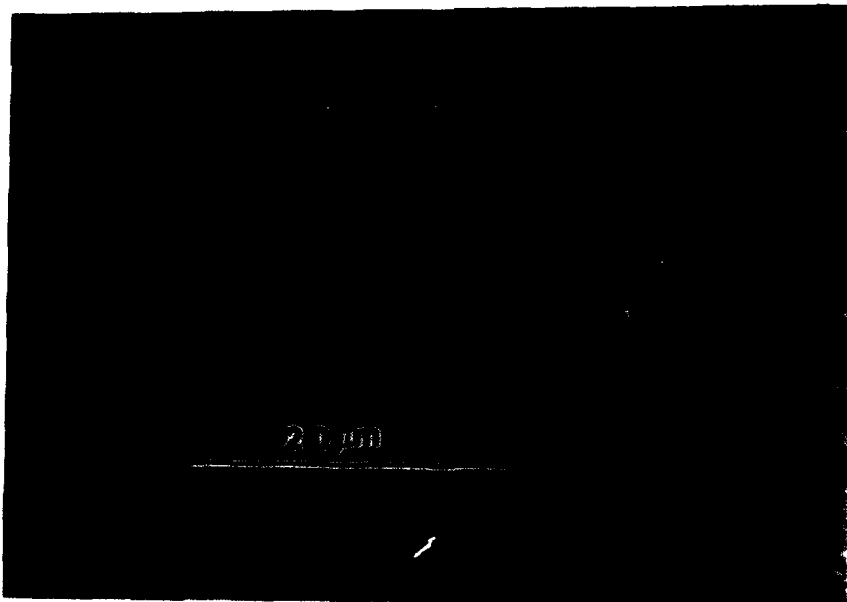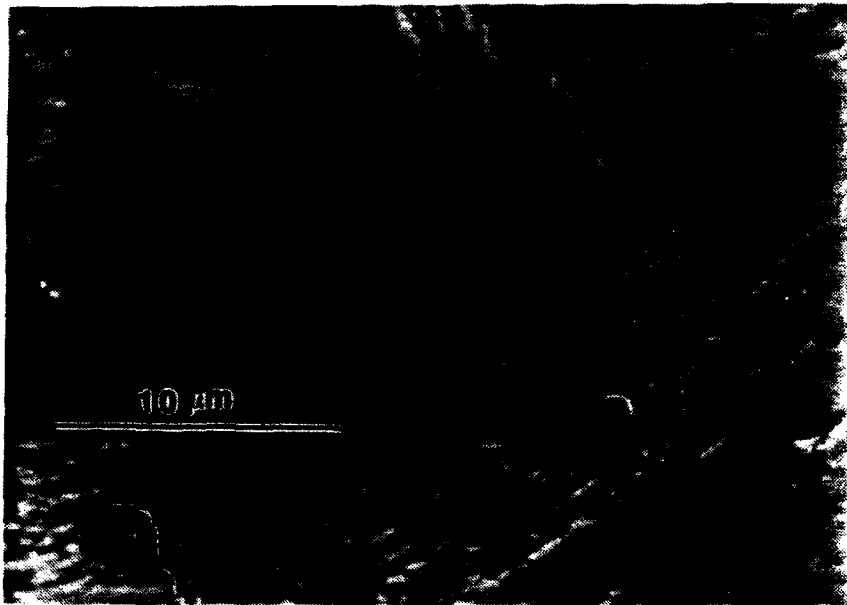
Figure 19
Top - SEM micrograph, magnification 3,770x; Bottom - SEM micrograph, magnification 2,000x.

47

1. TIG ULCB/ULCB 1.4MJ/m

The microstructures of the low heat input, ULCB/ULCB, TIG weldment are presented in Figures 20 and 21. The weld metal and heat affected zone (HAZ) microstructures both consist of large, widely dispersed, intragranular ferrite laths. The base metal microstructure is a combination of autotempered lath martensite and upper bainite.

2. TIG ULCB/ULCB 2.8MJ/m

The microstructures of the high heat input, ULCB/ULCB, TIG weldment are presented in Figures 22 and 23. This weldment possessed mechanical properties far superior to the other weldments. Quite evident in the weld metal microstructure are very distinct colony packets of fine, feathery upper bainitic ferrite along with intragranular acicular ferrite laths. The colony packets are an average size of $\sim 100\mu$m. The prior austenite grain boundaries are strongly decorated with granular ferrite. The HAZ is made up of an upper bainitic ferrite microstructure while the base metal is of a similar but coarser microstructure.

48
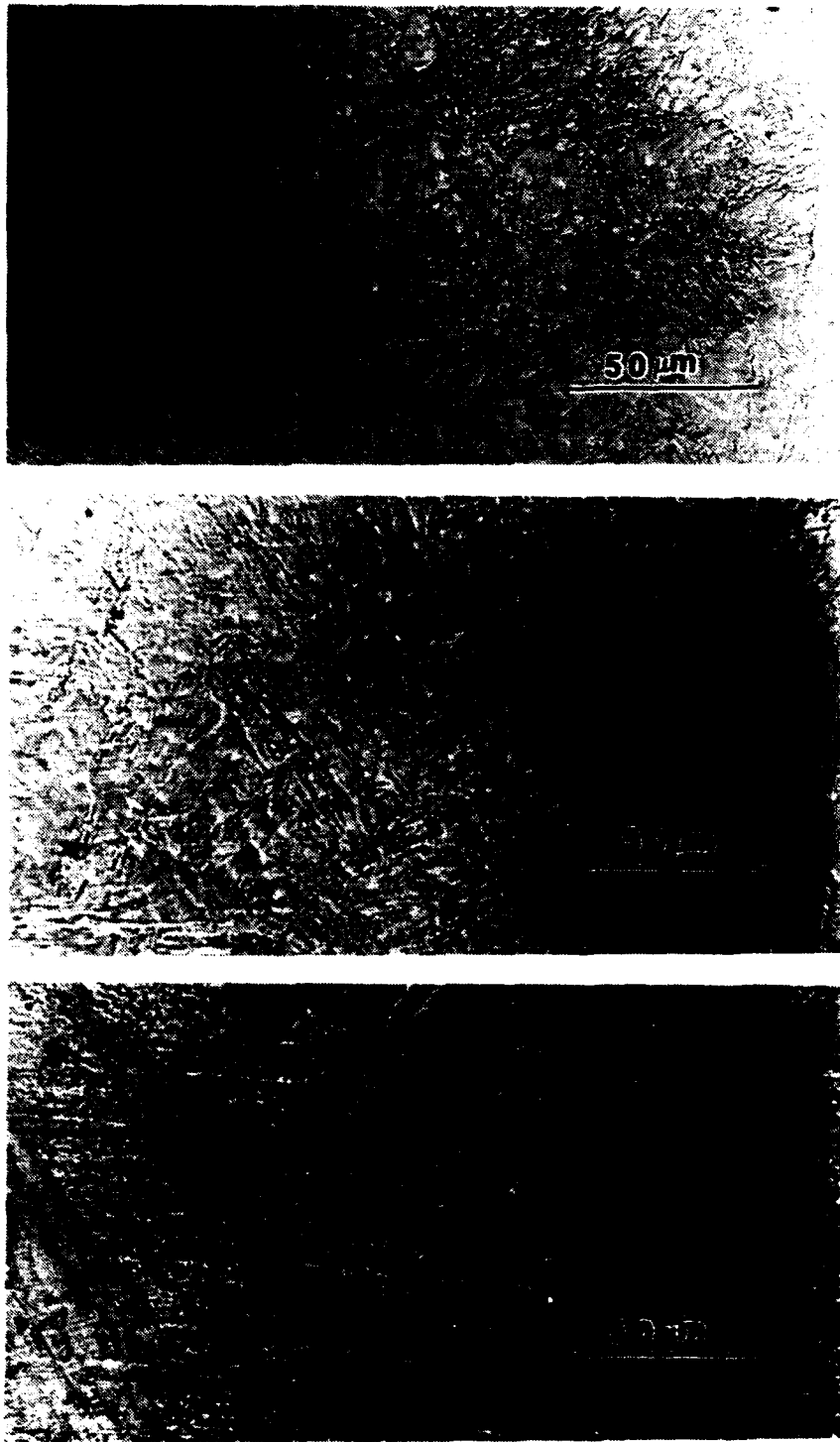
Figure 20
Optical micrographs for TIG, ULCB/ULCB, 1.4MJ/m weldment; (2% nital etch) 500x.
Top - weld metal; Middle - heat affected zone; Bottom - base metal.

49
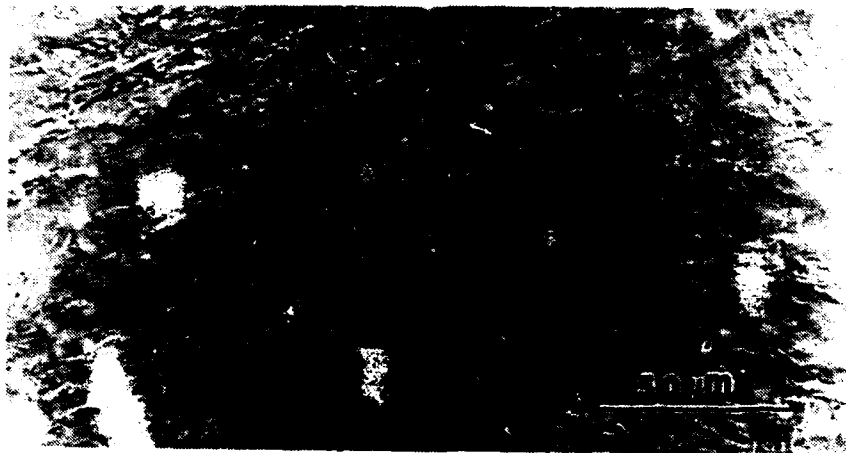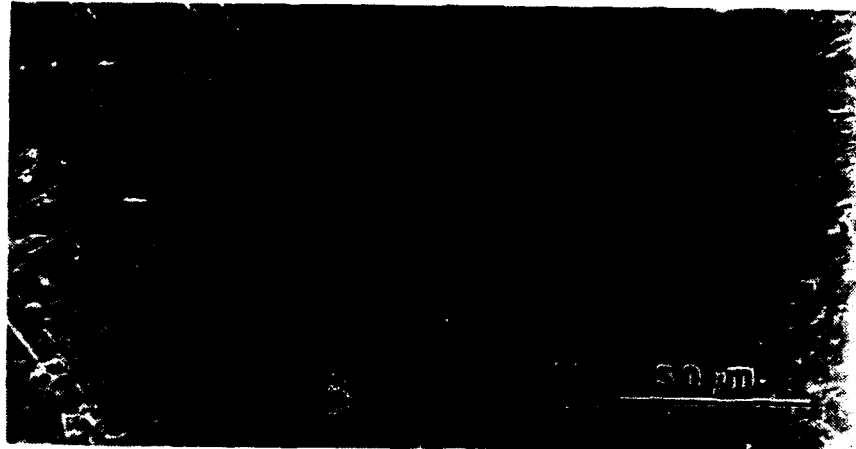
Figure 21

SEM micrographs for TIG, ULCB/ULCB, 1.4MJ/m weldment; (2% nital etch) 500x.
Top - weld metal; Middle - heat affected zone; Bottom - base metal.
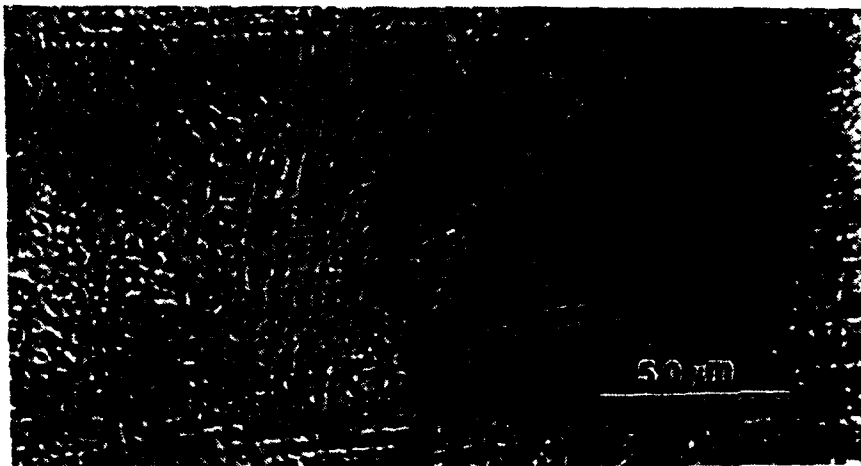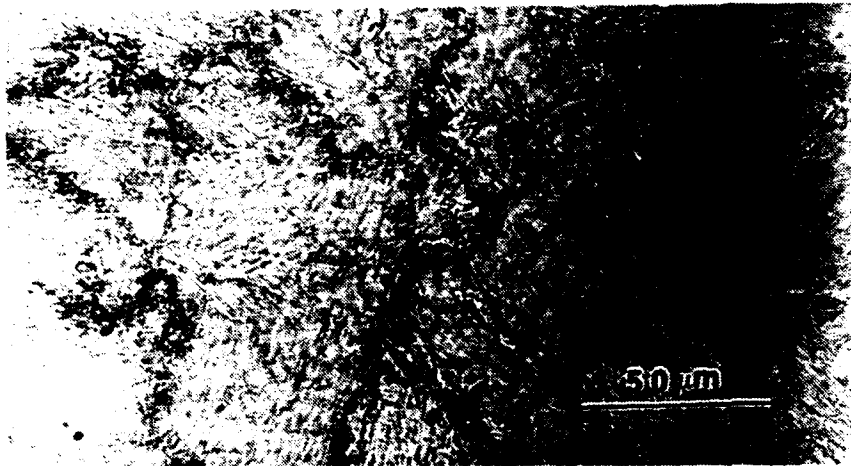
Figure 22

Optical micrographs for TIG, ULCB/ULCB, 2.8MJ/m weldment; (2% nital etch) 500x.
Top - weld metal; Middle - heat affected zone; Bottom - base metal.

51
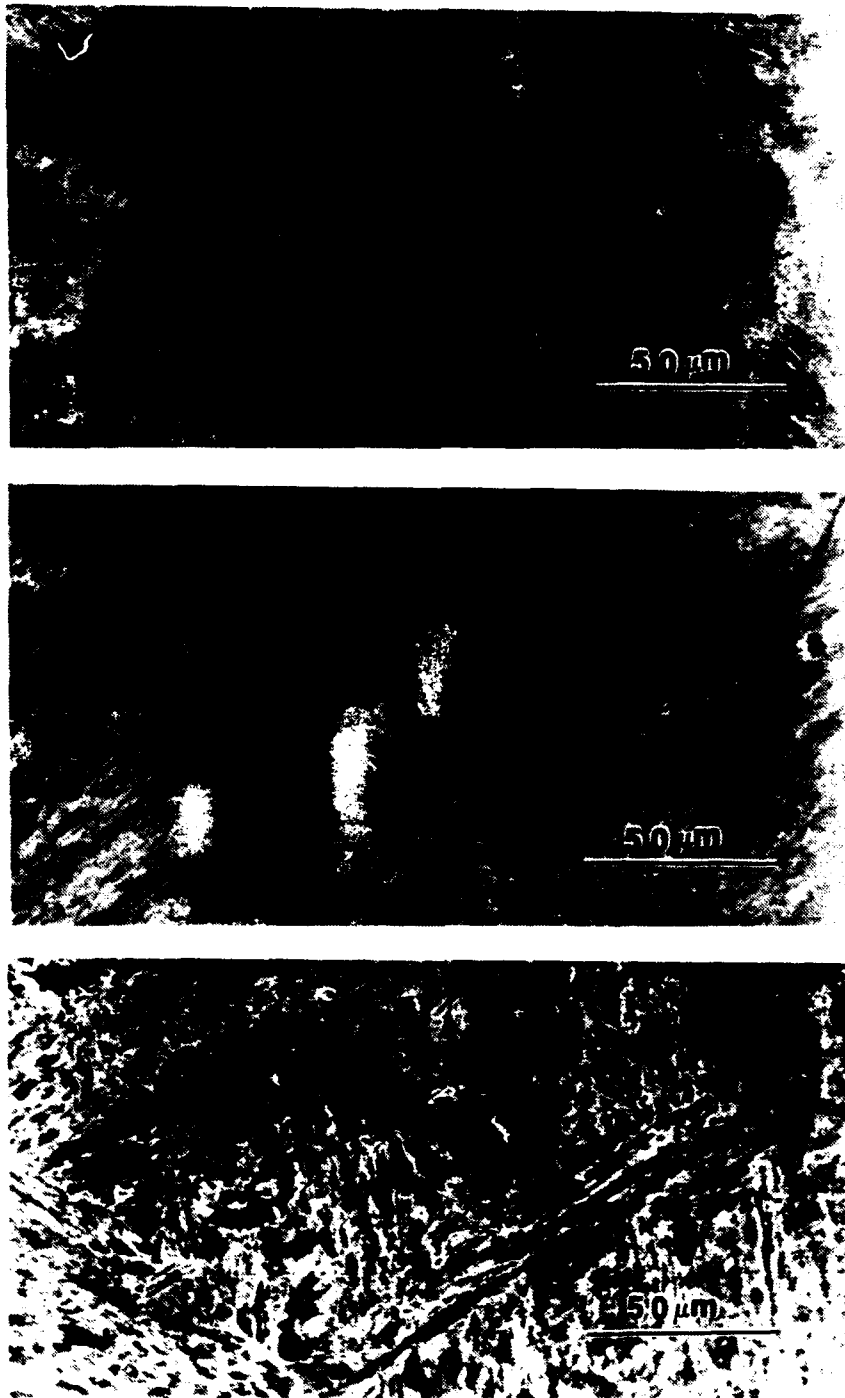
Figure 23
SEM micrographs for TIG, ULCB/ULCB, 2.8MJ/m weldment; (2% nital etch) 500x.
Top - weld metal; Middle - heat affected zone; Bottom - base metal.

3. TIG ULCB/HY-130 1.4MJ/m

The microstructures of the low heat input, ULCB/HY-130, TIG weldment are presented in Figures 24 and 25. The weld metal consists of colony packets of upper bainitic ferrite. The HAZ consists of a fine, feathery microstructure while the base metal is largely martensitic.

4. MIG ULCB/HY-130 1.4MJ/m

The microstructures of the low heat input, ULCB/HY-130, MIG weldment are presented in Figures 26 and 27. The microstructure largely consists of a fine, feathery, upper bainitic structure with a martensitic microstructure present in the base metal. This welding process introduced reactive cover gases and produced the poorest mechanical properties of the weldments studied. The effect of the reactive cover gases is discussed in the inclusion analysis to follow.
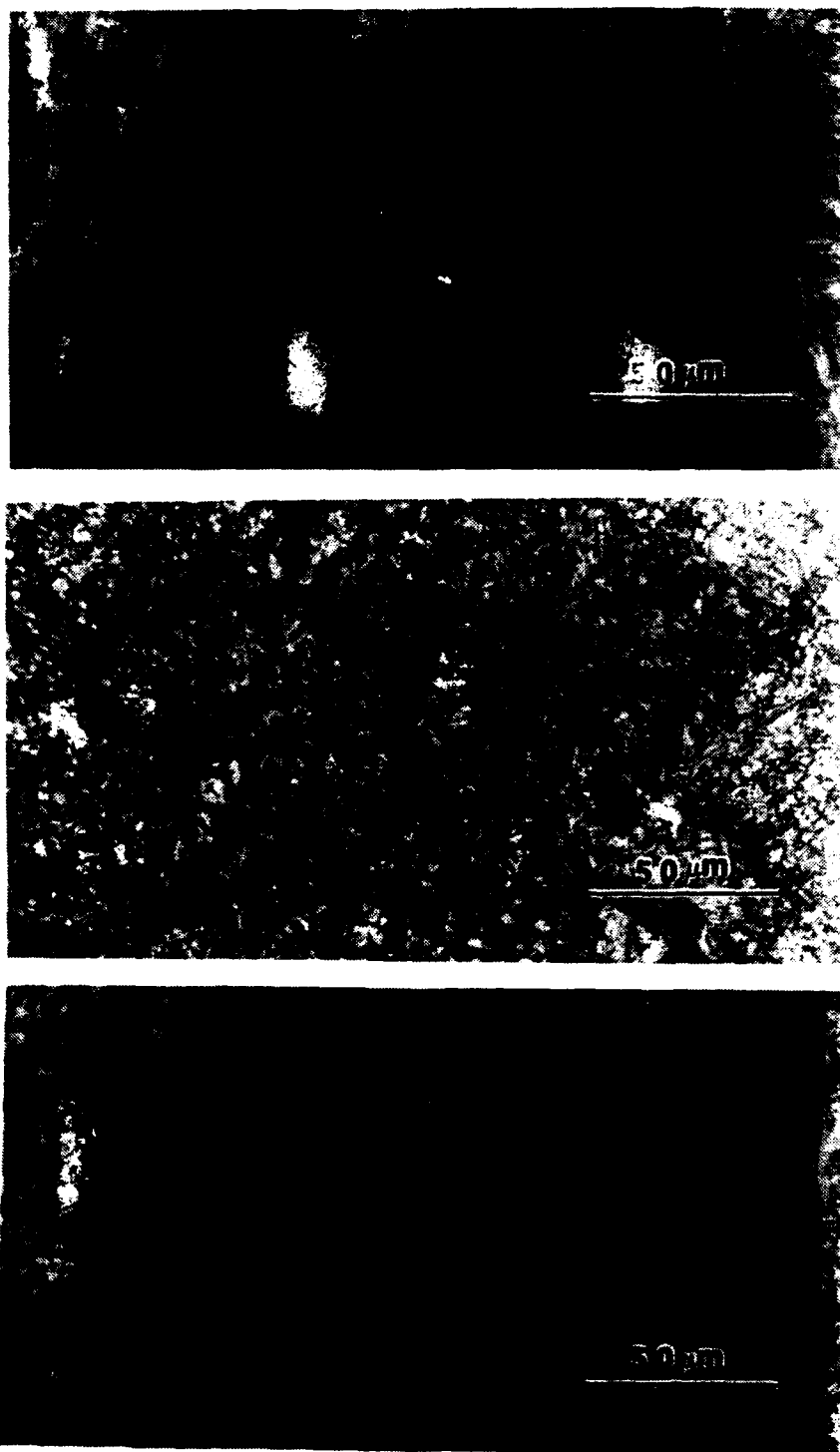
Figure 24

Optical micrographs for TIG, ULCB/HY-130, 1.4MJ/m weldment; (2% nital etch) 500x. Top - weld metal; Middle - heat affected zone; Bottom - base metal.
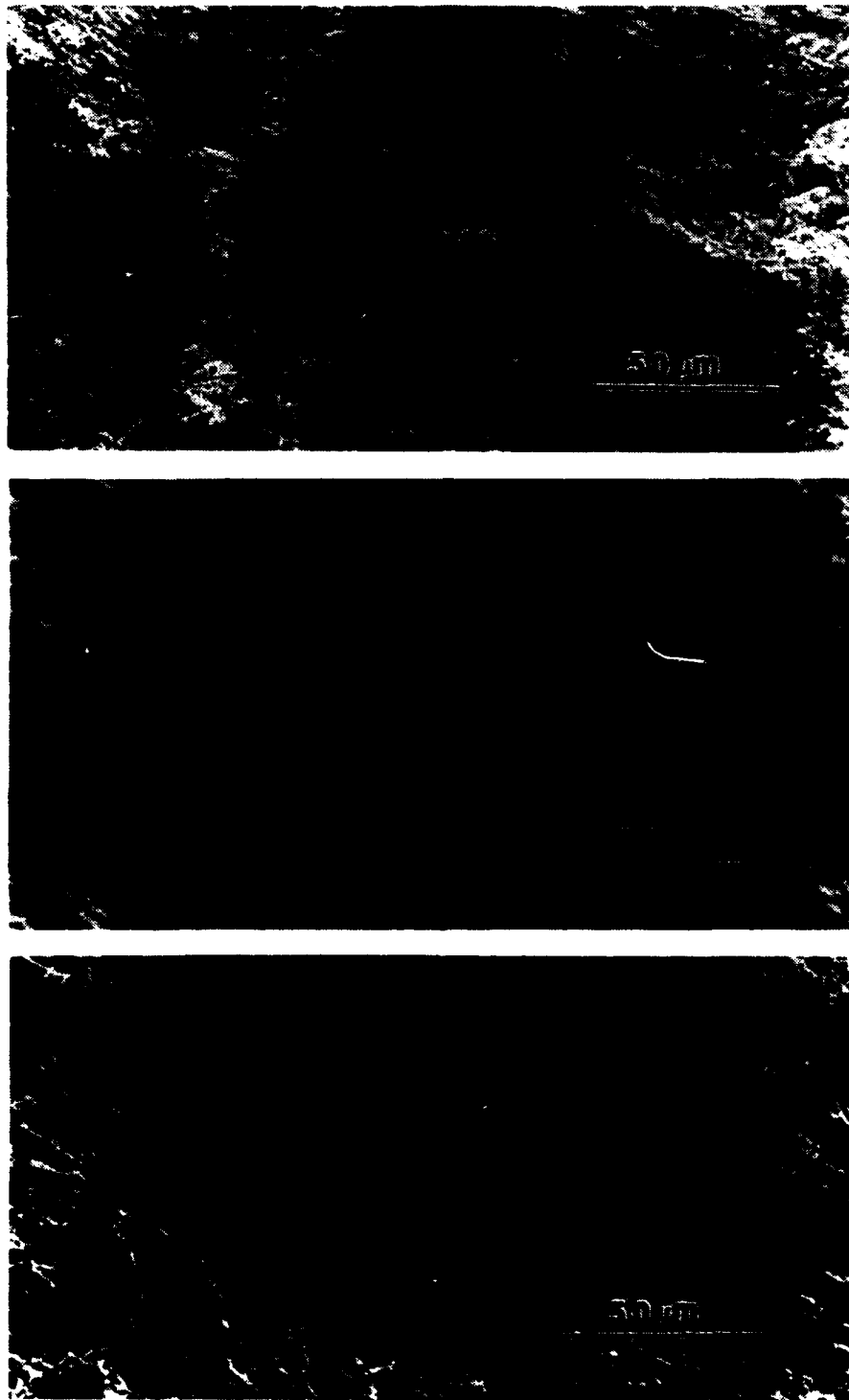
Figure 25

SEM micrographs for TIG, ULCB/HY-130, 1.4MJ/m weldment; (2% nital etch) 500x.
Top - weld metal; Middle - heat affected zone; Bottom - base metal.
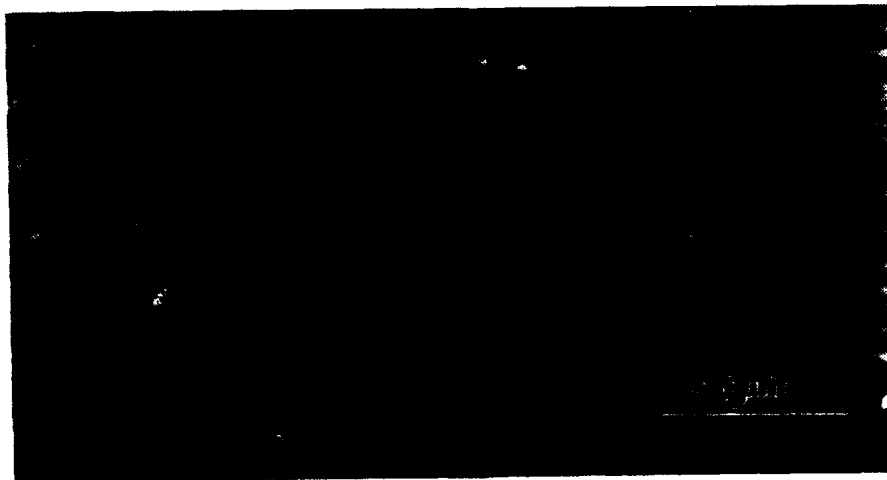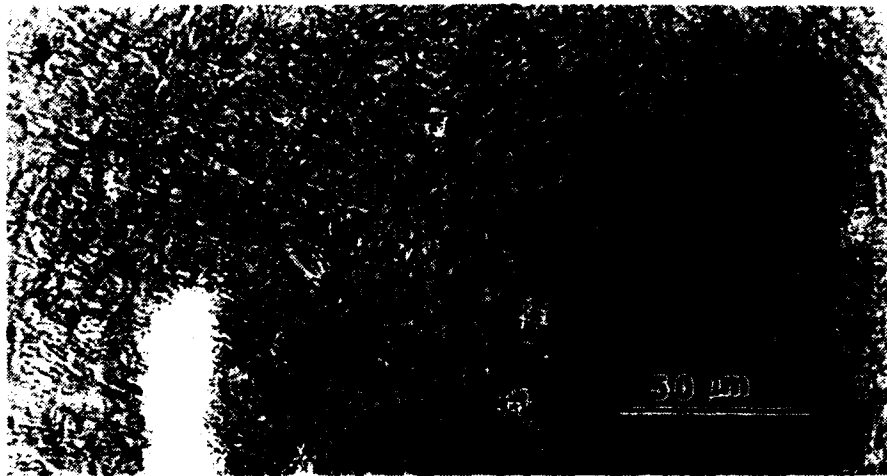
Figure 26

Optical micrographs for MIG, ULCB/HY-130, 1.4MJ/m weldment; (2% nital etch) 500x. Top - weld metal; Middle - heat affected zone; Bottom - base metal.

56
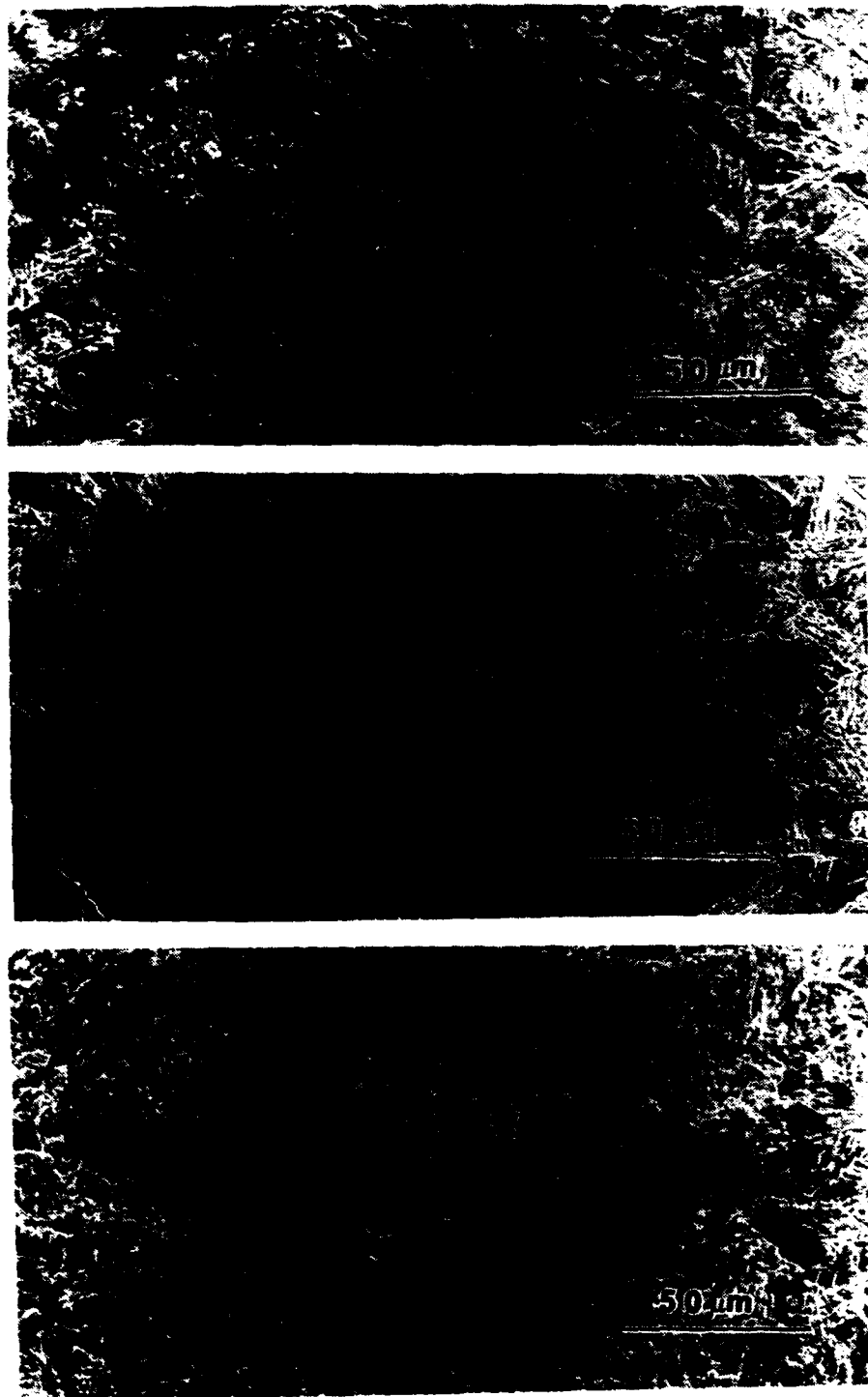
Figure 27

SEM micrographs for MIG, ULCB/HY-130, 1.4MJ/m weldment; (2% nital etch) 500x.
Top - weld metal; Middle - heat affected zone; Bottom - base metal.

57

D. INCLUSION ANALYSIS

1. Size/Quantity/Distribution

The inclusion frequency/size of the four weldments studied are presented in Figures 28 and 29. The vast majority of the nonmetallic inclusions identified were spherical. There is a notable difference in the frequency/size for the TIG weldments at the two different heat inputs (See Figure 28). The average inclusion size for the low heat input was 0.92μm and 0.37μm for the high heat input. Thus the inclusion size was reduced by a factor of two when the heat input rate was doubled. These inclusions were of sufficient size ($>0.2\mu$m) to promote the nucleation of acicular ferrite (Kiessling, 1989, p.106). However, the maximum cooling time for the weldments studied ($\sim$5s) was too rapid to effectively promote the nucleation of acicular ferrite (Grong, Matlock, 1986, p.37). Similar plots for the total number of inclusions as a function of size are presented in Figures 30 and 31. These figures are normalized to forty fields viewed at 2,000x magnification to illustrate the relative inclusion density associated with the four weldments studied. The quantity of inclusions roughly doubled when the heat input rate was increased by a factor of two (See Figure 30). The high heat input results in a longer weld pool retention time (reduced cooling rate). The average particle size was described in the Deoxidation of Steel Weld Metals section (See Figure 9) showing a sufficiently long reaction time results in reduced average particle size. The higher heat input provides more energy for the deoxidation reactions to occur generating a higher inclusion density.

58

INCLUSION FREQUENCY/SIZE
ULCB->ULCB TIG 1.4MJ/m

INCLUSION FREQUENCY/SIZE
ULCB->ULCB TIG 2.8MJ/m

Figure 28

INCLUSION FREQUENCY/SIZE
ULCB->HY130 TIG 1.4MJ/m

INCLUSION FREQUENCY/SIZE
ULCB->HY130 MIG 1.4MJ/m

Figure 29

60

INCLUSION QUANTITY/SIZE
ULCB->ULCB TIG 1.4MJ/m

INCLUSION QUANTITY/SIZE
ULCB->ULCB TIG 2.8MJ/m

Figure 30

61
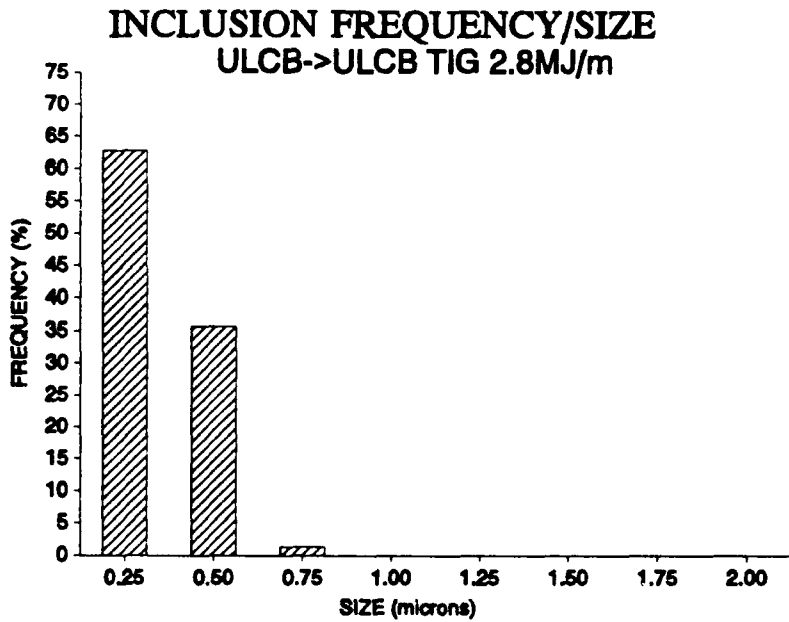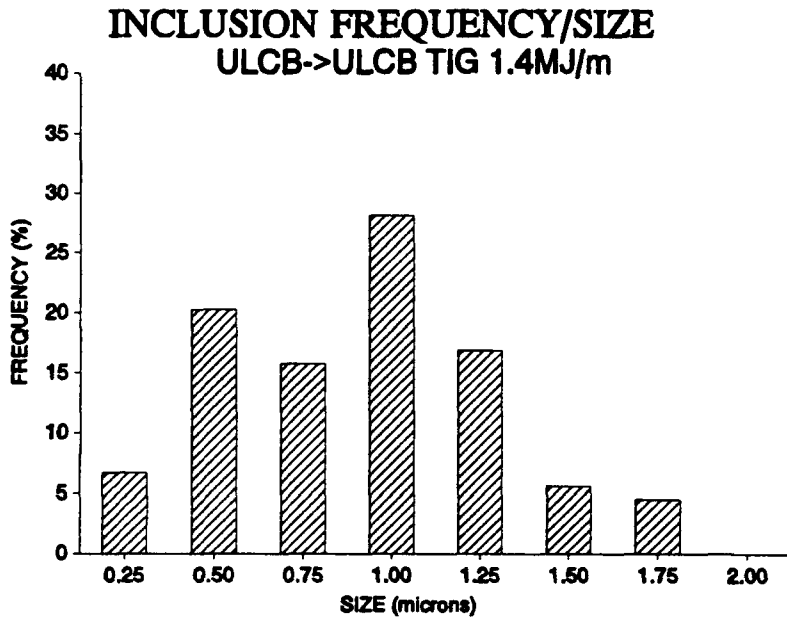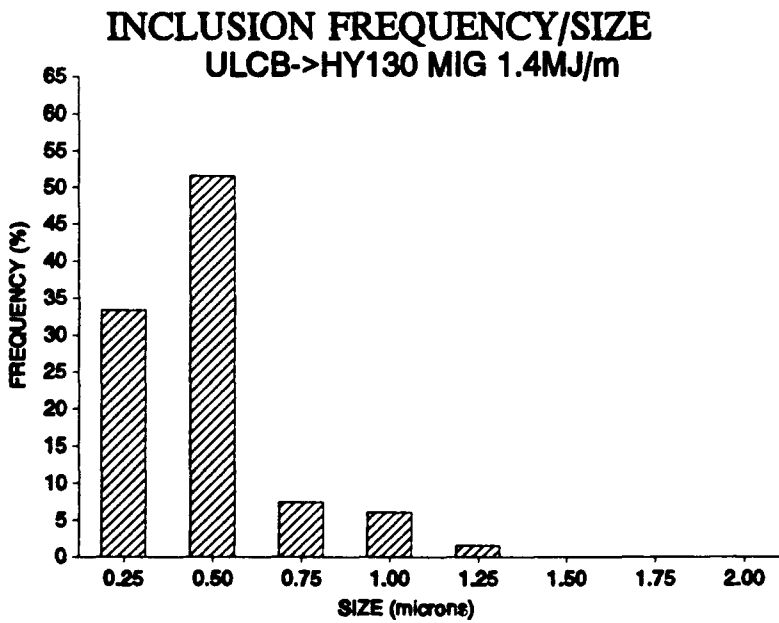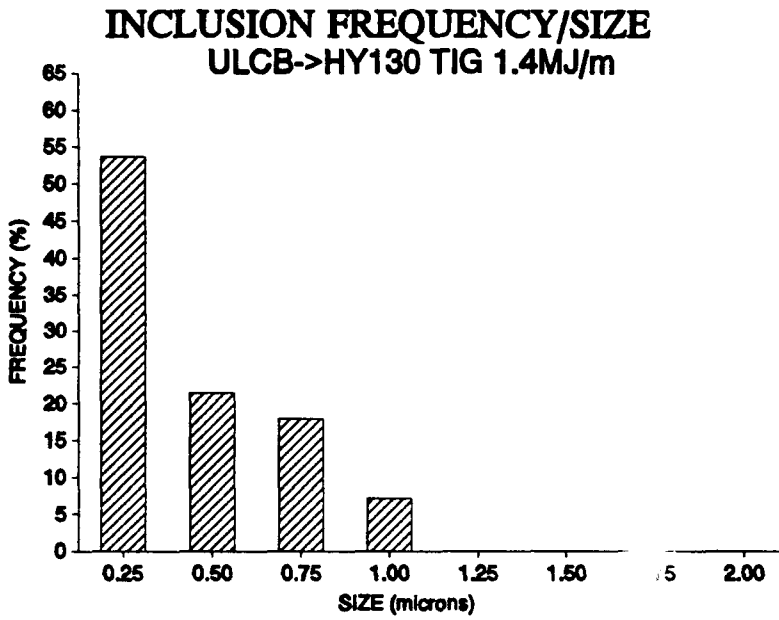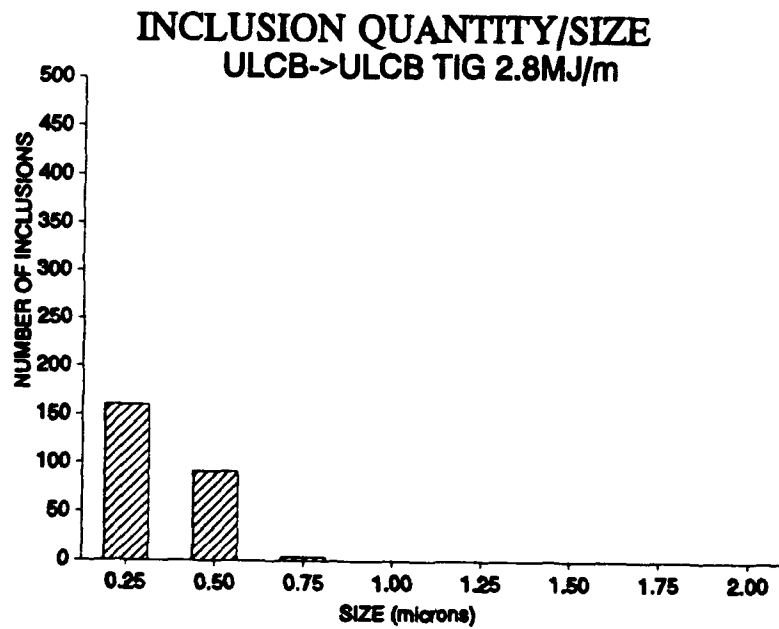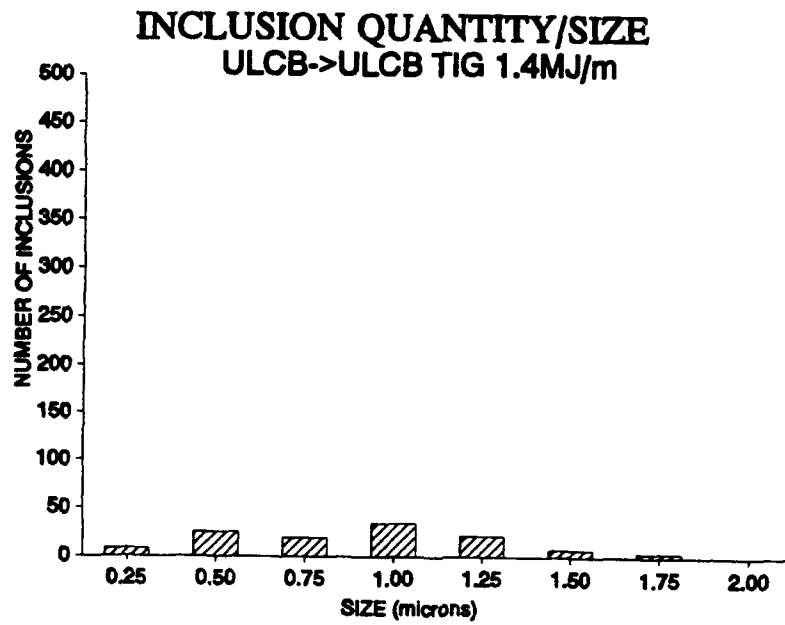
INCLUSION QUANTITY/SIZE
ULCB->HY130 TIG 1.4MJ/m
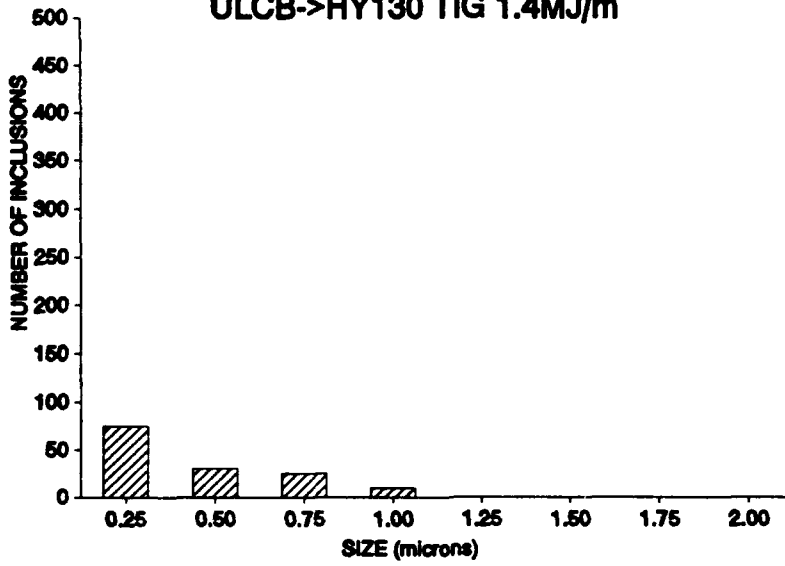
INCLUSION QUANTITY/SIZE
ULCB->HY130 MIG 1.4MJ/m
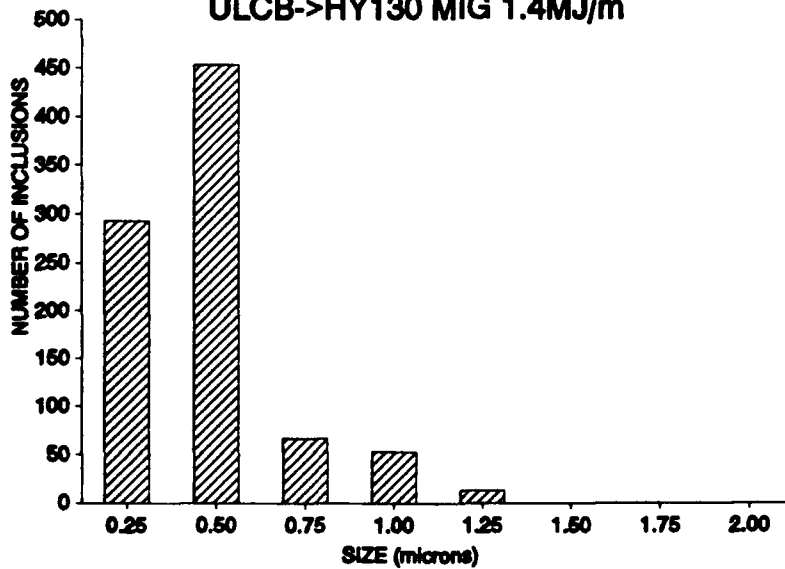
Figure 31

The MIG welding process utilized a M-5 cover gas containing 5% CO_2. These reactive gases along with the MIG welding process being "dirtier" than the TIG welding process (See Welding Methods Utilized in Analysis section) produced an enormous increase in the weld metal inclusion density. The inclusion density increased from approximately five inclusions per field to 25 inclusions per field (See Figures 30 and 31). Figure 32 illustrates a typical field associated with this MIG weldment. The TEM carbon extraction replica of the MIG weldment identified the formation of carbides. Figures 33 and 34 illustrate the presence of these carbides along with the spectral analysis. The large Cu peak present in Figure 34 and any subsequent spectral analyses comes from the copper wire mesh grids used in the preparation of the carbon extraction replicas and was therefore ignored. Spectral analyses which do not exhibit the Cu peak were produced using the more expensive beryllium grid. These carbides and the large increase in the inclusion density are no doubt responsible for the extremely poor mechanical properties of this weldment. The extremely brittle nature of the MIG weldment is evident in the percent elongation and percent reduction in area values presented in Table II.
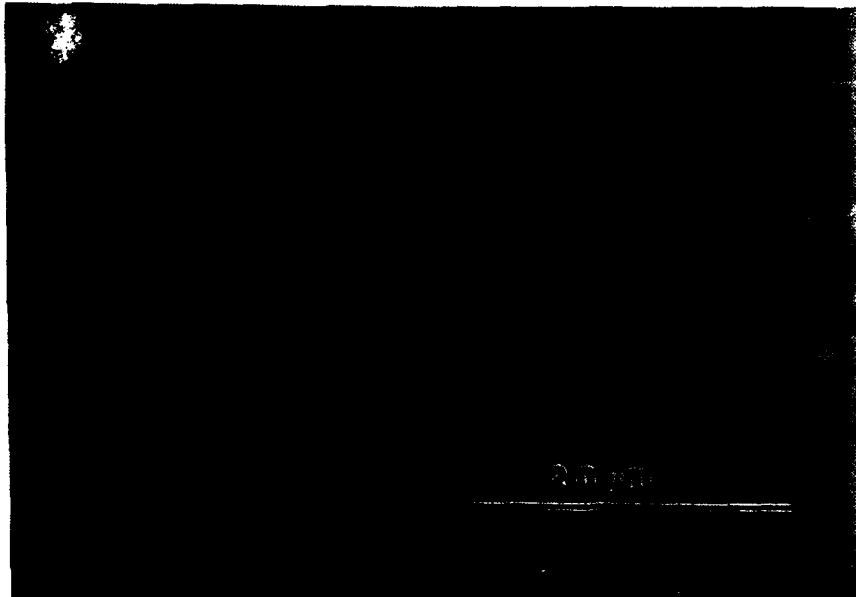
Figure 32
MIG weldment; ULCB/HY-130; 1.4MJ/m; backscattered electrons; magnification 2,000x.
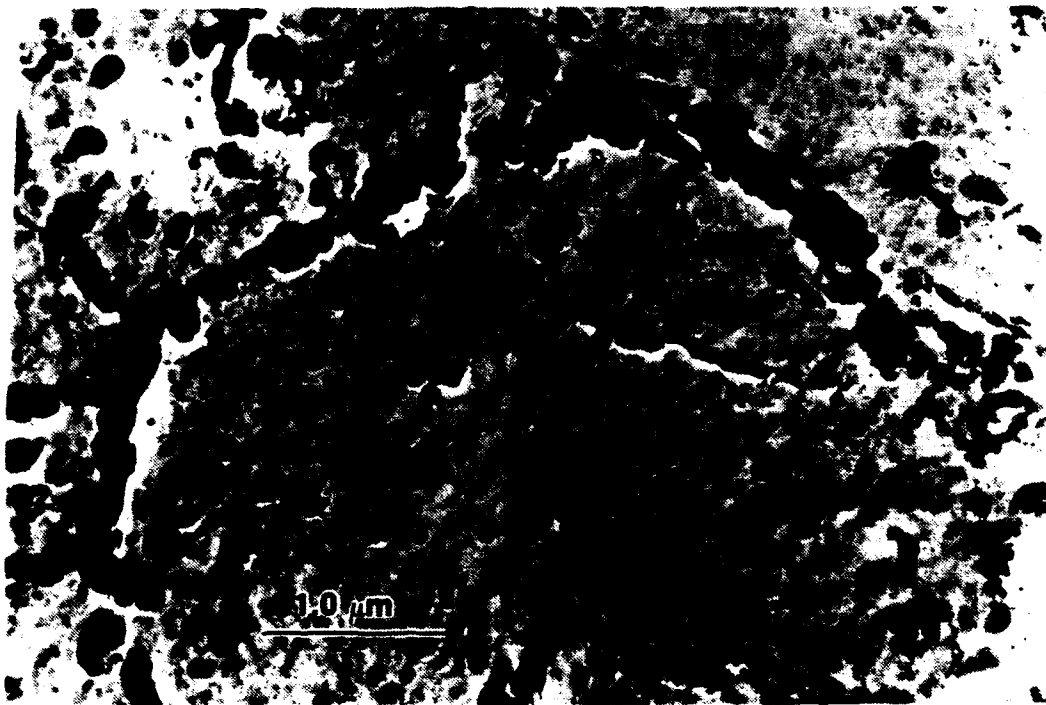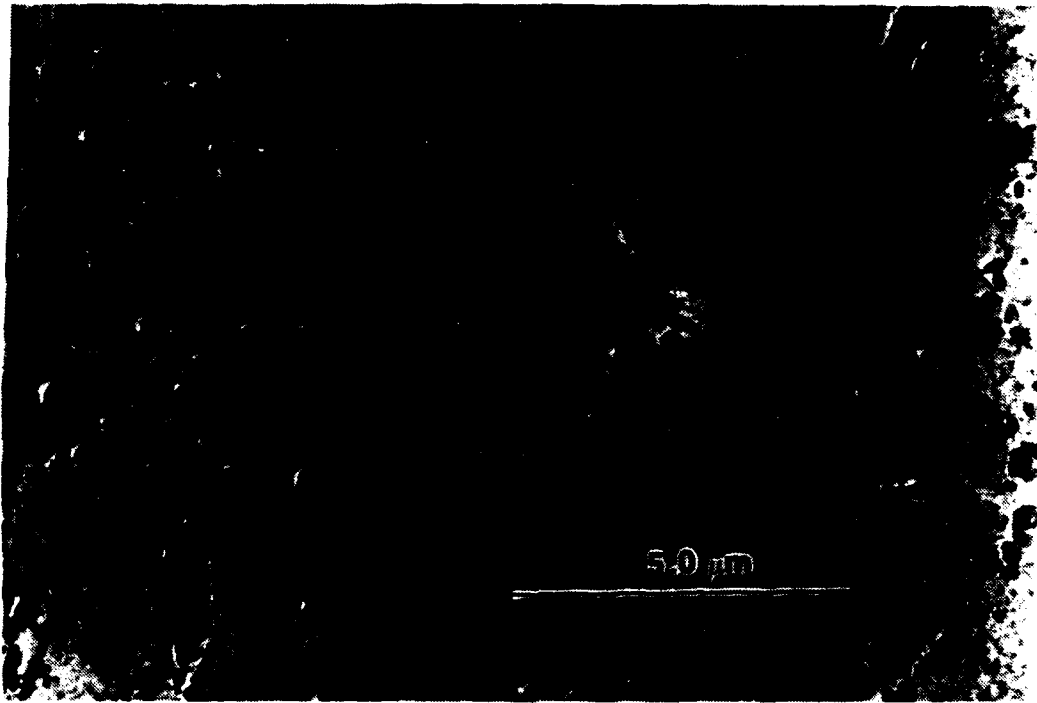
Figure 33
Formation of carbides in MIG, ULCB/HY-130, 1.4MJ/m weldment. Carbon extraction replica. Top - 8,000x; Bottom - 24,000x.
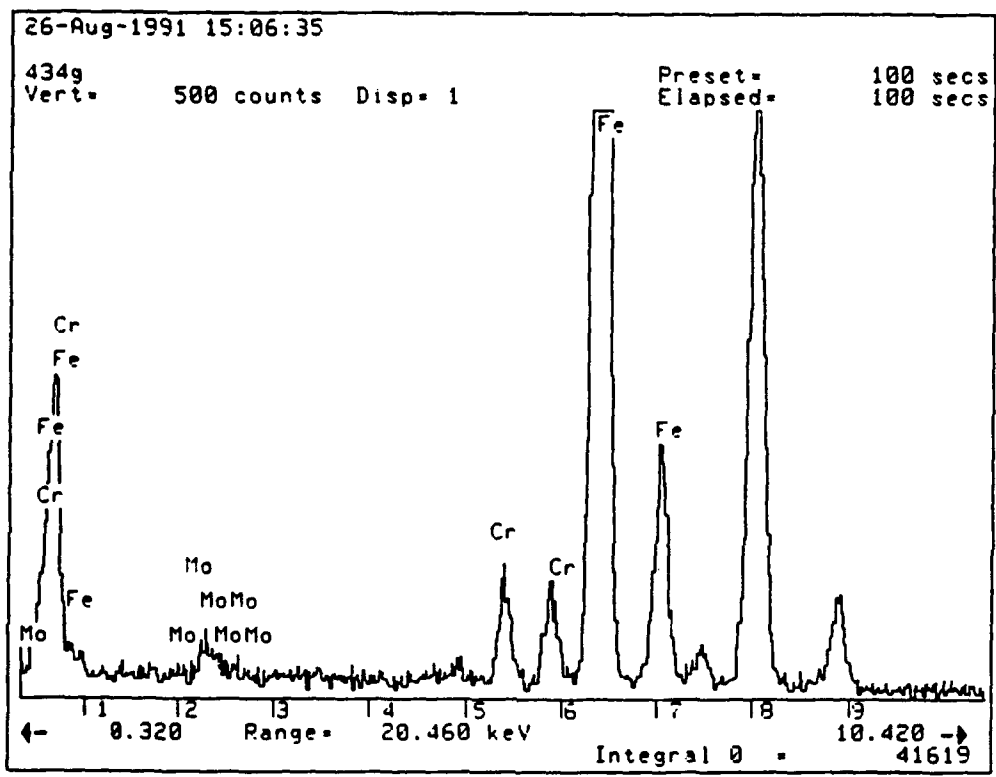
Figure 34
Spectral analysis associated with carbide formation in MIG weldment.

66

2. Composition

The chemical composition of the nonmetallic inclusions was originally performed using the KEVEX analyzer in conjunction with the scanning electron microscope. However, significant errors were introduced in the normalizing and matrix stripping routine associated with spectral analysis using the SEM. Considerable ambiguity was introduced with the Molybdenum L-peaks coinciding with the K-α Sulfur peak. Carbon extraction replicas were produced suitable for TEM thin foil analysis thus eliminating many of the problems encountered with the SEM spectral analysis. Based on chemical composition, several different types of inclusions were identified containing the following elements:

Al, Si, S, Ti, Cr, Mn, and Mo

The majority of the inclusions were complex aluminum-silicates or manganese-aluminum-silicate materials. The inclusions were "glassy" showing no evidence of a diffraction pattern. The bulk of the inclusions belonged to one of the following groups:

$MnO-SiO_2-Al_2O_3-TiO_2$

$SiO_2-Al_2O_3$

$MnO-Al_2O_3-SiO_2$

MnS

The following figures are a representative sample of the major groups of inclusions identified along with the associated spectral analyses.
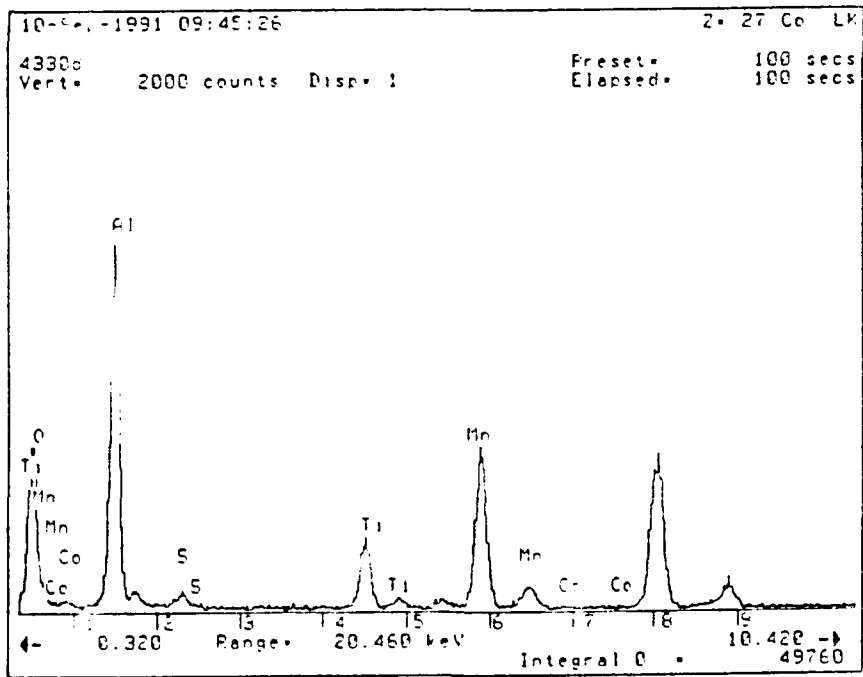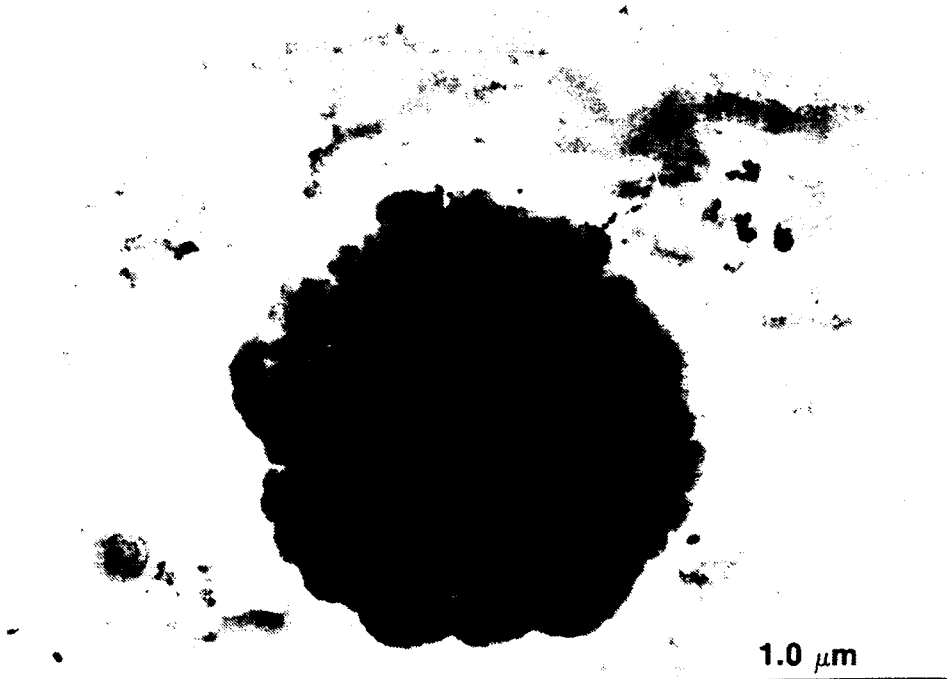
Figure 35
Carbon extraction replica: magnification 40.000x.
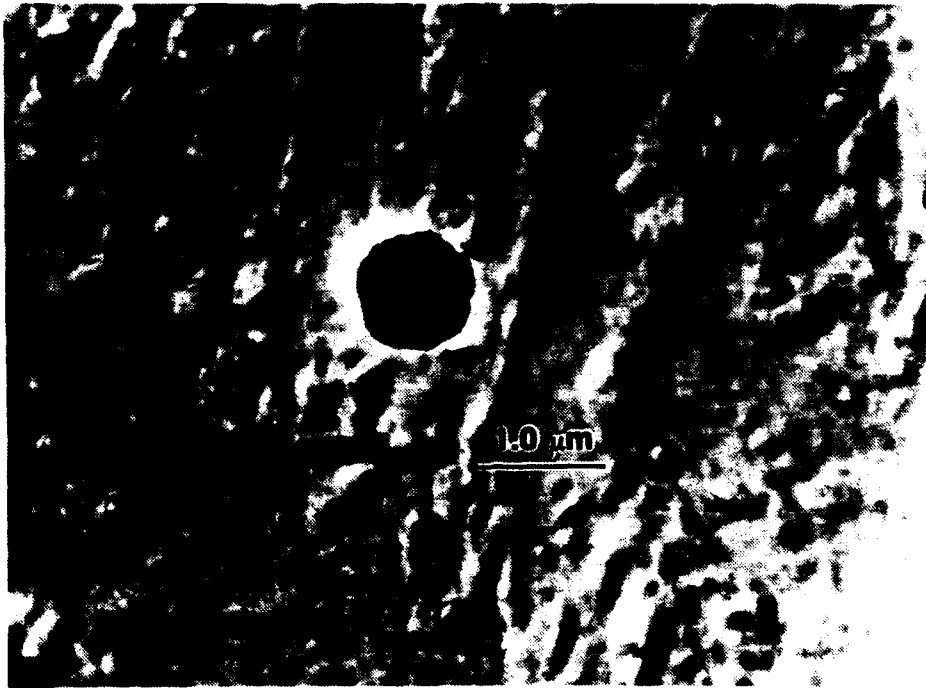
Figure 36
Carbon extraction replica; magnification - top 17,000x; bottom 53,000x.
Composition presented in Figure 37.

69
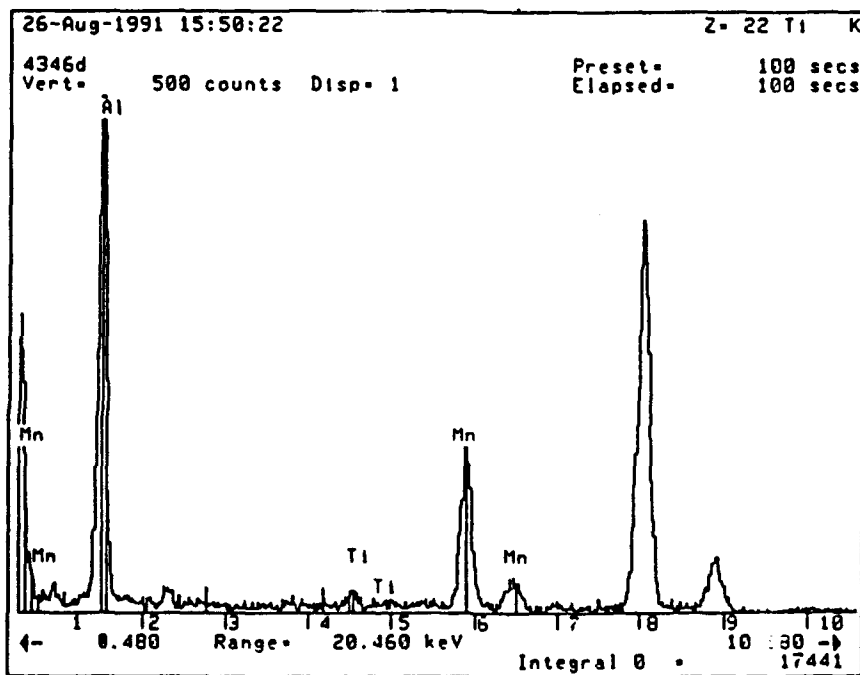
Figure 37
Spectral analysis for Figure 36.

70
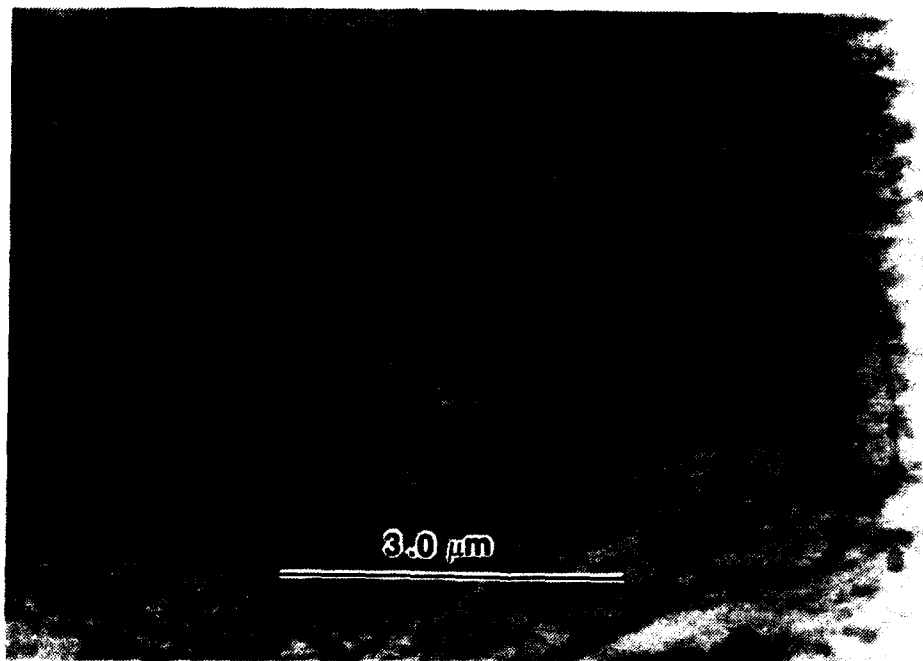
Figure 38
Carbon extraction replica; magnification 14,000x.
Composition presented in Figure 40.

71
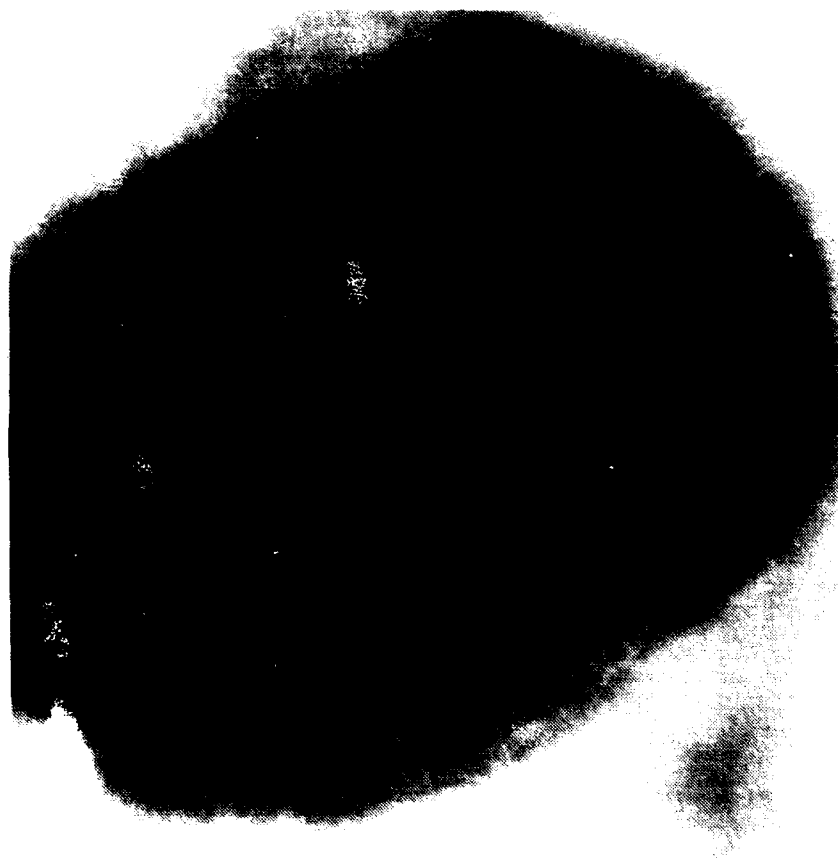
0. 5 μm

Figure 39
Carbon extraction replica; magnification 130,000x.
Composition presented in Figure 40.
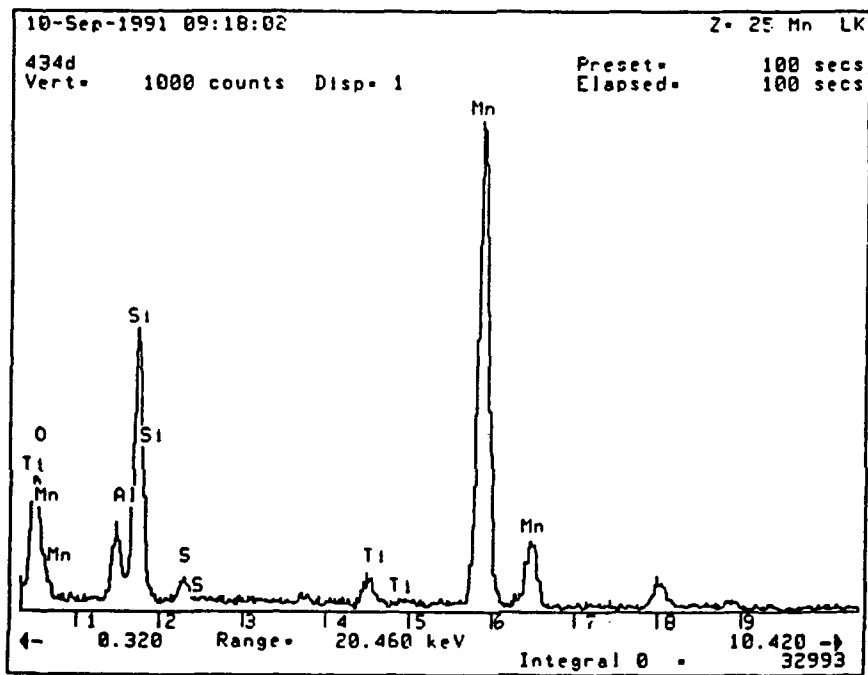
Figure 40
Spectral analysis for Figures 38 and 39.

73
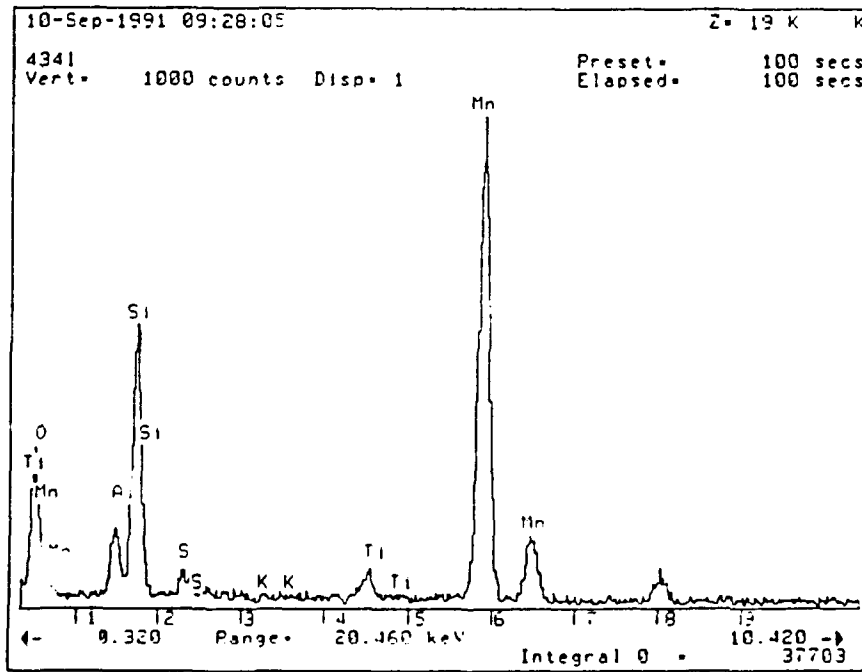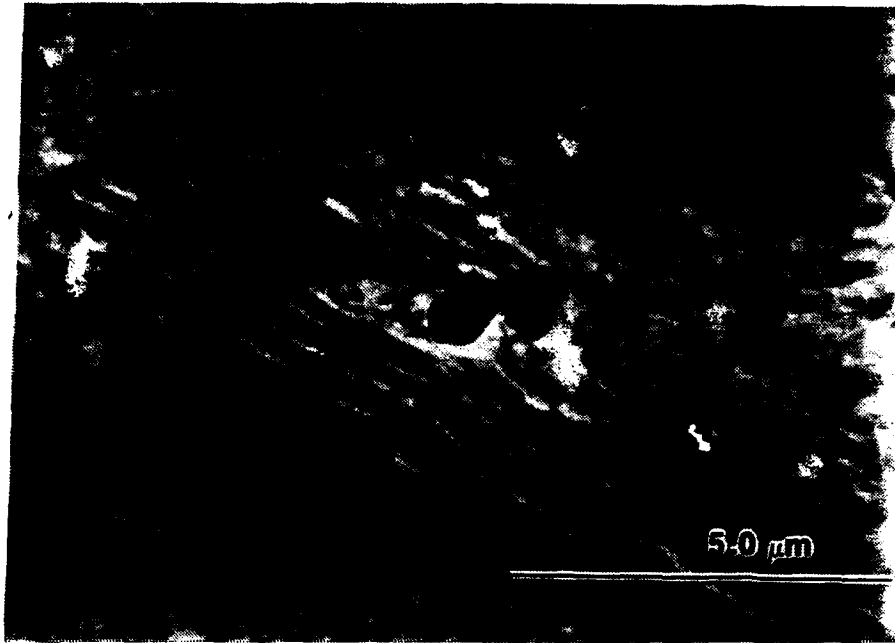
Figure 41
Carbon extraction replica; magnification 9,000x.

74
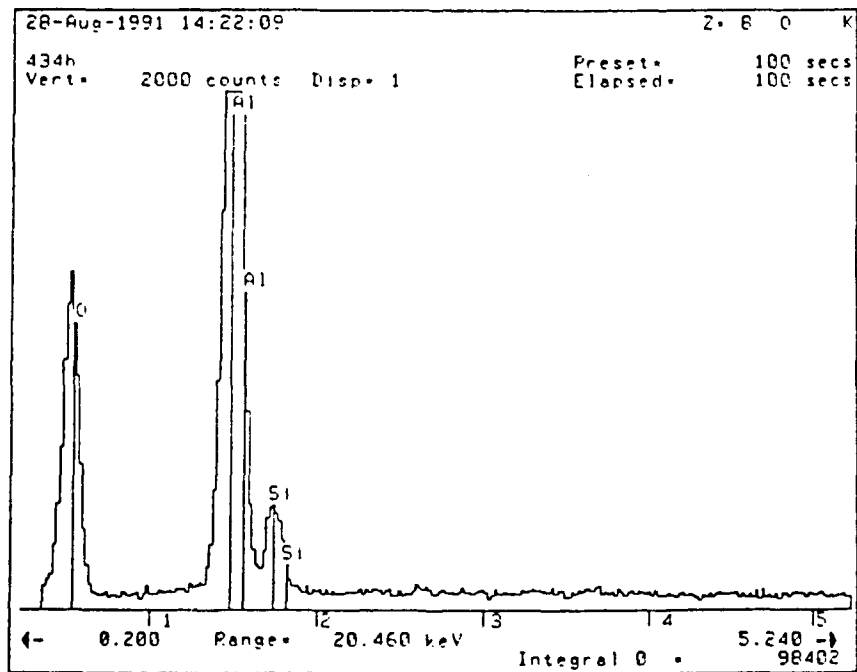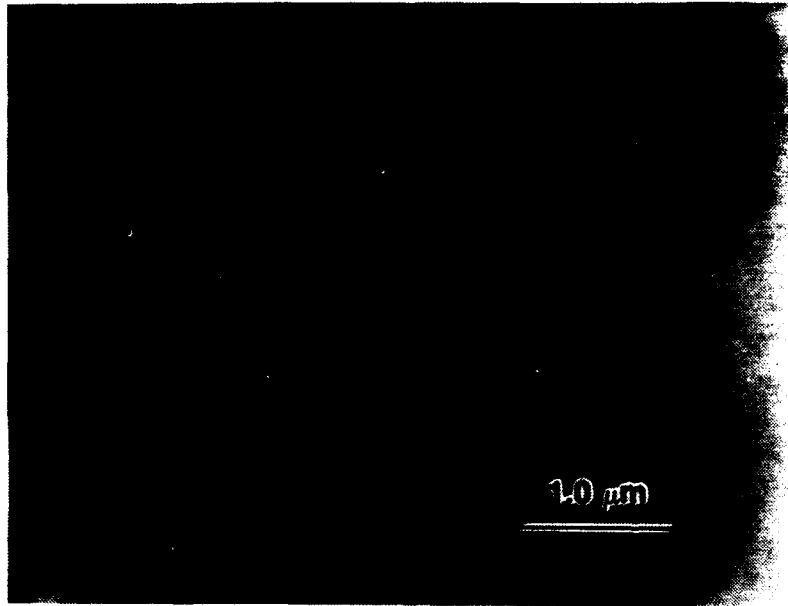
Figure 42
Carbon extraction replica; magnification 20,000x.

75
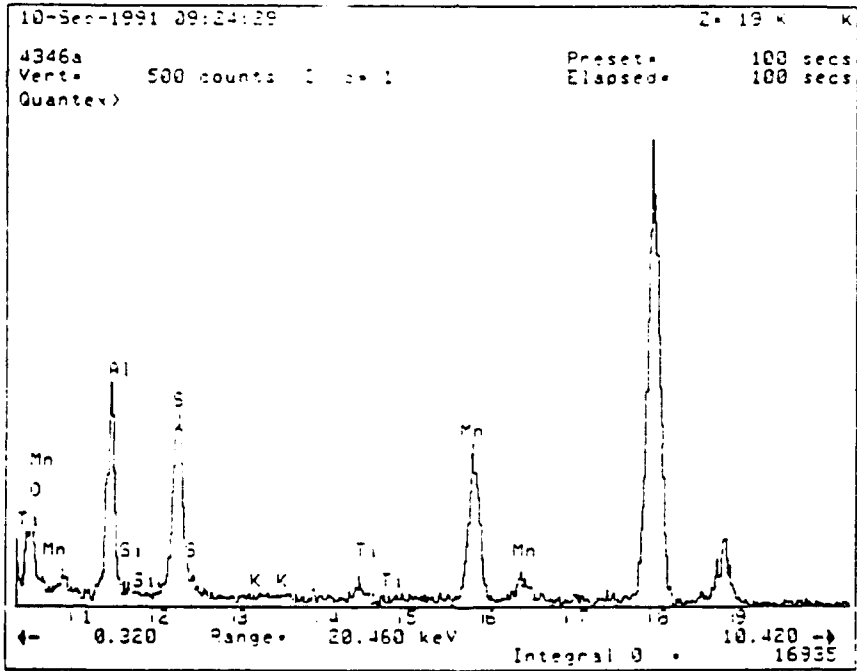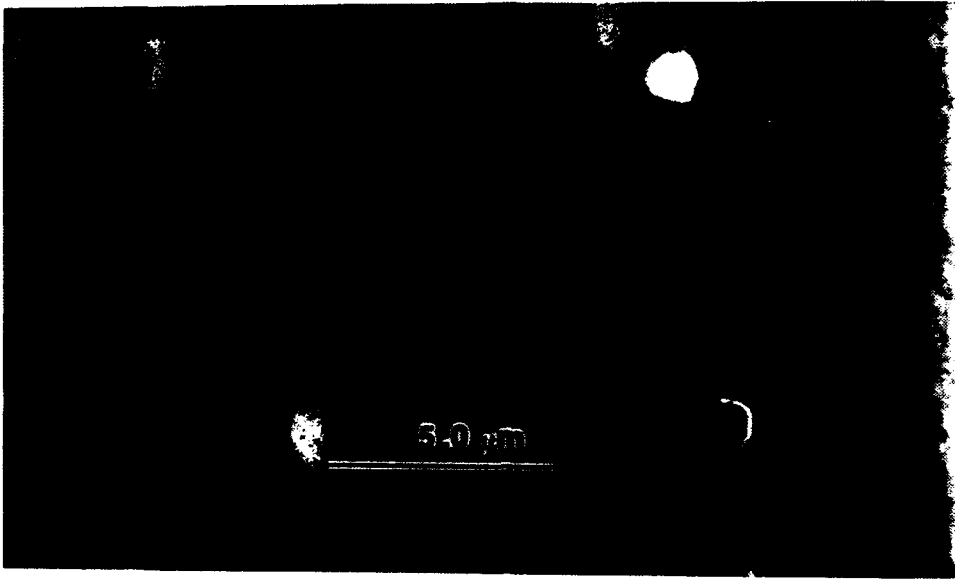
Figure 43
Carbon extraction replica; magnification 6,000x.

10-Sep-1991 09:49:11

4338a
Vert= 1000 counts Disp= 1

Preset=   100 secs
Elapsed=   100 secs
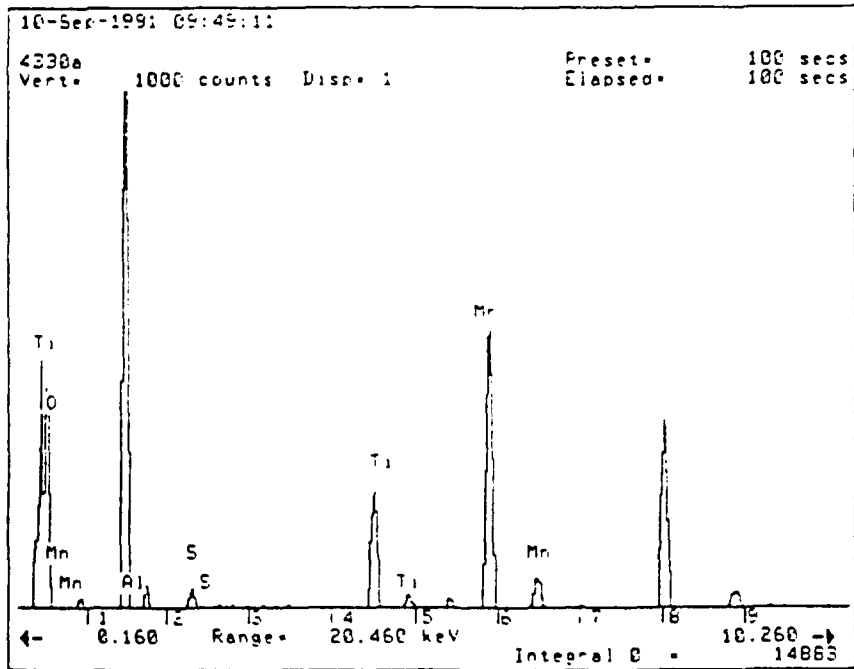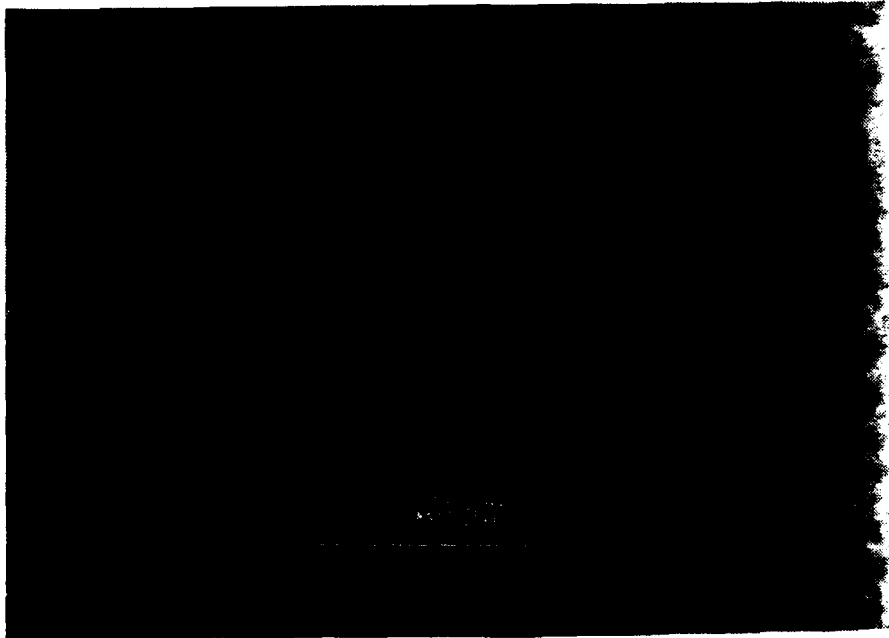
Figure 44
Carbon extraction replica; magnification 36,000x.

The analysis of the EDX data was performed using the atomic/molar percent of each identified element. The inclusion type was determined based on established stoichiometries and the appropriate phase diagrams. The following illustrative example pertains to the inclusion presented in Figures 38 and 39.

THIN FILM ANALYSIS
(THEORETICAL K-FACTORS)

Accelerating voltage   120.0 KeV

Beam - sample incidence angle   90.0 degrees

Xray emergence angle   74.3 degrees

Xray - window incidence angle   2.3 degrees

Element & Line	Weight Percent	Atomic Percent	Precision # 2 Sigma	Intensities
Al Ka	3.97	6.57	0.53	33.87
Si Ka	17.94	28.52	1.24	167.62
S Ka	1.86	2.59	0.39	15.87
Ti Ka	2.93	2.73	0.61	22.71
Cr Ka	0.40	0.34	0.24	2.88
Mn Ka	72.90	59.24	3.58	492.19
Total	100.00			

ABSOLUTE PRECISION OF WEIGHT PERCENT

Figure 45
Inclusion elemental make-up.

Based on established stoichiometries the weight percent of MnO, Al_2O_3 and SiO_2 was calculated to be 53.7, 7.6 and 39.8 percent respectively. The phase diagram (See Figure 46) indicates the complex inclusion falls into the Rhodonite region which has a low melting point ($\sim 1200°C$) and is therefore glassy.
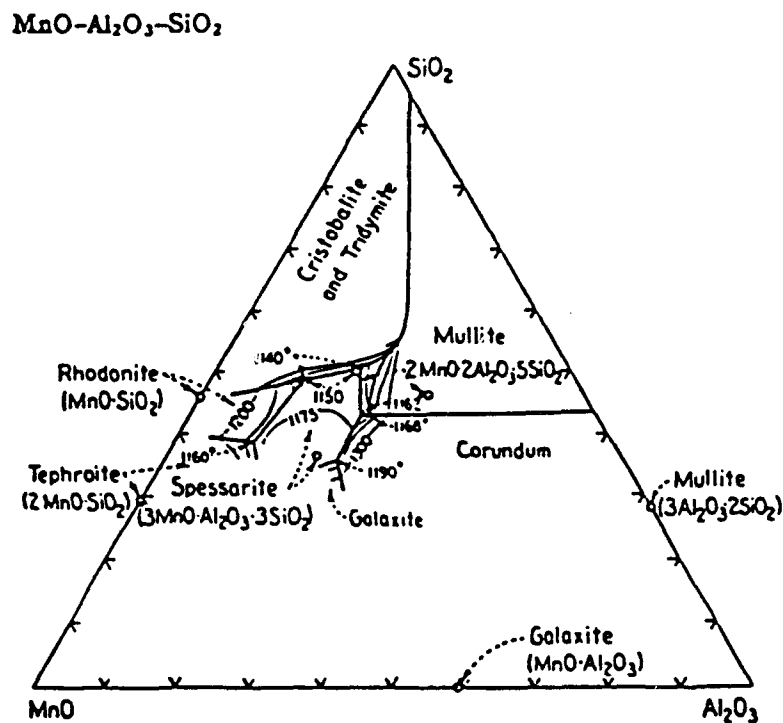
$MnO-Al_2O_3-SiO_2$

Figure 46
Phase diagram for $MnO-Al_2O_3-SiO_2$ system (Levin et al., 1964, p.252).

79

A second illustrative example pertains to the inclusion presented in Figure 42.

This is a binary oxide made up of aluminum and silicon.

THIN FILM ANALYSIS
(THEORETICAL K-FACTORS)

Accelerating voltage   120.0 KeV

Beam — sample incidence angle   90.0 degrees

Xray emergence angle   74.3 degrees

Xray — window incidence angle   2.3 degrees

Element & Line	Weight Percent	Atomic Percent	Precision # 2 Sigma	Intensities
Al Ka	91.76	92.06	2.30	933.49
Si Ka	8.24	7.94	0.69	91.88
Total	100.00			

ABSOLUTE PRECISION OF WEIGHT PERCENT

Figure 47
Inclusion elemental make-up.

Based on established stoichiometries the weight percent of Al_2O_3 and SiO_2 was calculated to be 90.6 and 9.4 percent respectively. The binary phase diagram (See Figure 48) indicates this inclusion belongs dominantly to the Corundum family.
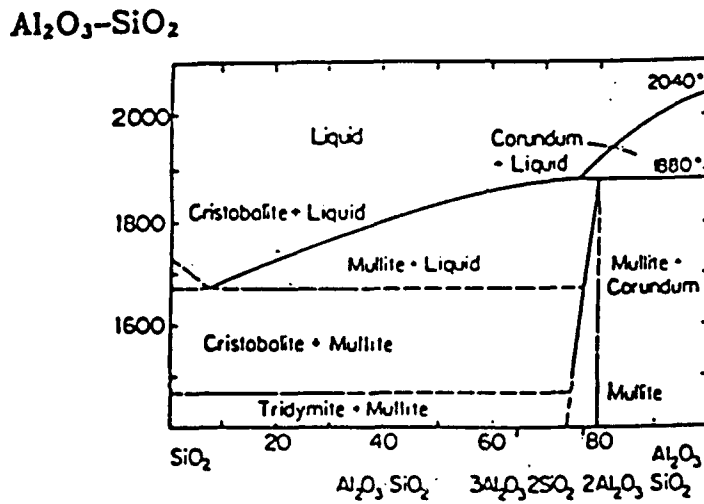
Al_2O_3–SiO_2

Figure 48
Binary phase diagram for Al_2O_3-SiO_2 system (Levin et al., 1964, p.122).

Overall, there was no significant compositional segregation of nonmetallic inclusions throughout the weldments.

81

V. SUMMARY

A. CONCLUSIONS

1. Weld Metal Heat Input

The mechanical properties of the ULCB steel weldments were largely dependent on the heat input rate. The high heat input (2.8MJ/m) for the ULCB/ULCB steel weldment resulted in a tough, finely grained macrostructure with superior mechanical properties whereas the low heat input (1.4MJ/m) produced a much weaker columnar/dendritic growth. This macrostructural development was attributed to the degree of constitutional supercooling associated with the level of heat input and subsequent cooling rate.

2. Base Plate Composition

The mechanical properties of the two ULCB steel weldments utilizing the HY-130 base metal were inferior to those utilizing ULCB steel base plates. This was attributed to carbon pickup from the HY-130 base metal occurring in the fusion zone.

3. Reactive Cover Gas

The MIG weldment utilizing a reactive cover gas had the poorest overall mechanical properties. The presence of a reactive cover gas markedly increased the inclusion density as well as promoting the formation of carbides.

4. Microstructure

The major factor determining the microstructure of the as-deposited weld bead was the heat input rate. The microstructures of the ULCB steel weldments were largely upper bainitic with some evidence of inclusion nucleated ferrite laths. However, the macrostructural effects appeared to be dominant over the influence of the microstructure on the toughness of the weldments.

5. Nonmetallic Inclusions

The majority of all the nonmetallic inclusions identified were spherical, complex aluminum-silicates or manganese-aluminum-silicates. The average inclusion size was reduced by a factor of two when the heat input rate was doubled going from $0.92\mu m$ for the low heat input to $0.37\mu m$ for the high heat input. The number of inclusions roughly doubled when the heat input rate was increased by a factor of two. The presence of nonmetallic inclusions did not appear to be dominant in the nucleation of acicular ferrite or in controlling the microstructural development. Although the inclusions present were of sufficient size ($>0.2\mu m$) to promote the nucleation of acicular ferrite, the cooling time of all of the weldments studied largely remained in the region favoring the formation of a martensitic/bainitic microstructure.

B. RECOMMENDATIONS FOR FUTURE STUDY

The influence of weld metal composition and cooling rate determines the degree of constitutional supercooling and thus the final macrostructure. Future study involving the accurate determination of the temperature gradient present in the weld pool and the

associated influence on macrostructural development would illuminate the degree of supercooling required to achieve the desired macrostructures. Conversely, for a fixed heat input the composition changes the equilibrium temperature associated with the weld metal and influences the degree of constitutional supercooling by shifting the "upper" curve (See Figure 16). The presence of numerous, small nonmetallic inclusions was generated through the use of a reactive cover gas. Studies involving the variation of heat input to extend the cooling time in conjunction with the presence of a high inclusion density may yield a tough weld metal if the proper combination of cooling rate and inclusion density are achieved to stimulate the nucleation of acicular ferrite.

APPENDIX A

SCANNING ELECTRON MICROSCOPY

The Scanning Electron Microscope (SEM) was used as the initial step in evaluating

the size, distribution and composition of the nonmetallic inclusions. A variety of images

and signals are generated by the SEM, each offering valuable information.

The secondary electron (SE) mode provides topographical information through the

collection of low energy secondary electrons, typically $\leq$ 50 eV. Secondary electrons

are generated from fast incident electrons colliding with and ejecting a lightly bound

valence electron. Since they have little energy, secondary electrons can escape from the

sample only if they are near the surface. High surface contours and rises allow more

secondary electrons to escape and thus produce a bright image. Conversely, crevices

restrict the escape of secondary electrons and appear dark. Regions of high atomic

number emit more secondary electrons and appear bright. Lastly, regions of low

resistivity accumulate charge and produce bright images while conductive regions are

darker. This is beneficial in identifying foreign objects on the sample surface.

The backscattered electron (BSE) mode was used exclusively for the identification

of nonmetallic inclusions. Backscattered electrons are produced from elastic or nearly

elastic collisions of incident electrons with the nucleus of a target atom. The BSEs are

much more energetic than the secondary electrons and therefore escape from deeper

within the sample. These high energy electrons are used for atomic number or

orientation information. The higher the atomic number of an atom, the greater the positive charge of its nucleus. Production of a BSE is more likely to occur and be of higher energy for a large positively charged nucleus. Low atomic number elements show up dark since fewer electrons are backscattered and those that are backscattered have lower energies. Thus, the backscattered electrons may identify the phases present in an inclusion by variations in contrast.

Energy dispersive x-ray analysis was performed using the SEM in conjunction with the KEVEX analyzer. Incident electrons of sufficient energy may collide with an atom and eject an electron from a low energy shell. This vacancy is filled by an electron within the atom losing energy through the emission of electromagnetic radiation. This emitted x-ray is characteristic of the target element involved and is collected by a detector. The resulting signals are analyzed by the KEVEX analyzer to identify the element and the relative amount present.

APPENDIX B

ENERGY DISPERSIVE X-RAY SPECTROSCOPY

When incident electrons of sufficient energy bombard a specimen in the SEM or TEM an electron from the inner shell of a sample atom may be ejected. The ejected electron leaves the atom with an inner shell vacancy (unstable state). The resulting ion is said to be in an "excited" state. An electron from a higher-energy shell will undergo transition to fill the vacancy and return the atom to its normal ground state. In dropping to a state of lower energy, the electron gives up some of its energy in the form of electromagnetic radiation. The atom may emit an x-ray photon characteristic of the element present and the transition producing the x-ray. Qualitative and quantitative analysis of these x-rays was performed by the KEVEX analyzer.

Inclusion spectrum data was collected at a nominal count rate of approximately 1500 cps for a period of 100 seconds. This resulted in a dead time of approximately seven percent. The working distance was set at 18.0 mm in the SEM. The spectra were analyzed using a matrix stripping routine. The background spectrum was normalized based on two "windows". The Fe L-peak and the flat region of the spectrum from 3 keV to 4 keV were painted as windows. The normalizing procedure looks at each channel in the painted region and computes the ratio of the spectrum intensity to the intensity of the background. This information is the basis for normalizing the entire background to be consistent with the level of the spectrum being analyzed.

Several restrictions apply to the energy dispersive x-ray micro-analyzer. The electrons only penetrate the sample surface slightly and thus do not represent the bulk composition of the sample. The x-ray signal has poor spatial resolution compared to the secondary and backscattered electron signals since the x-rays travel much greater distances through the sample than the electrons and leave the sample from depths at which the primary electron beam has widely spread. Light elements (Z < 11) are difficult to detect with energy dispersive x-ray analysis since the x-rays produced from light elements have low energy (long wavelength) and encounter difficulty penetrating the detector window. The EDX detector has poor efficiency below Z=11. Also, light elements have a low fluorescent yield (favor production of Auger electrons over x-rays) and thus produce fewer x-rays resulting in a weaker signal.

Quantitative analysis was performed using ZAF corrections:

1. Z - accounts for the effect of the atomic number on excitation efficiency, fluorescent yield, and detector efficiency.

2. A - incorporates the absorption of x-rays within the sample and detector, accounting for the probability of an x-ray being detected once it is generated.

3. F - evaluates the contribution to spectrum peaks from excitation of sample elements by x-rays generated within the sample; x-ray induced fluorescence.

Thin foil analysis using the KEVEX analyzer in conjunction with carbon extraction replicas in the TEM eliminated many of the difficulties introduced by the presence of the matrix metal during SEM EDX analysis.

APPENDIX C

PREPARATION OF CARBON EXTRACTION REPLICAS

The Ernest F. Fullam Vacuum Deposition Unit (VDU) was used for the preparation of carbon extraction replicas. One carbon rod was sharpened to a point of diameter 1-2mm. The other rod was prepared in the EFFA Carbon Rod Sharpener to achieve a thin rod protrusion of at least 5mm. This protrusion evaporates and deposits on the sample. The rod with the protrusion was fed into the stationary carbon rod through the spring tension associated with the rod holder apparatus (See Figure 48). A vacuum of approximately 10 microns mercury was established in the VDU and a current of 45-50 amps was applied to reach the evaporation temperature of carbon. The evaporation process takes between 10 and 60 seconds depending on the integrity of the contact between the carbon rods. Glass slides were used to isolate the region of interest by covering the unwanted areas. The slides also served as an indicator of the film thickness by comparing them to a standard thickness scale. The carbon deposition process was repeated to achieve the desired thickness of 200-300 Å. A dark blue carbon film is desired but some success was achieved with a thinner gold tone film. The surfaces of the coated samples were scribed into small squares (approximately 3mm x 3mm) and then immersed in a 5% nital solution. The film became grayish in color and after five minutes most of the scribed regions floated off the sample or peeled partially from the surface. The samples were transferred to a beaker with methanol to remove the

89

remaining foils. At this point, the foils were warped and curled. The foils were then transferred to a beaker of water with 20 volume percent acetone. The surface tension of this solution flattened the foils. The flattened foils were removed from the water-acetone mixture using small 150 mesh Beryllium grids and 400 mesh Copper grids. Beryllium grids were preferred over copper grids as the copper grids interfered with EDX analysis on the TEM. This procedure yielded many useful samples suitable for TEM observation.
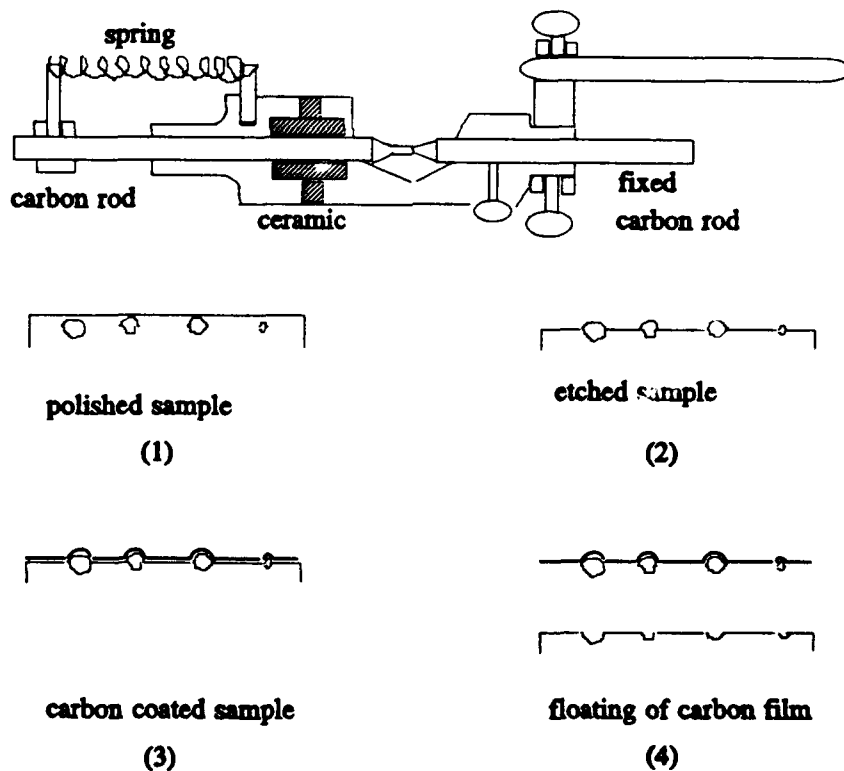

Figure 49

Carbon rod holder apparatus along with basic steps in obtaining a carbon extraction replica.

LIST OF REFERENCES

Abson, D.J., Dolby, R.E. and Hart, P.H.M., "The role of non-metallic inclusions in ferrite nucleation in carbon steel weld metals," International Conference on Trends in Steel and Consumables for Welding, The Welding Institute, London, 13-16 November 1978.

Abson, D.J., Pargeter, R.J., "Factors influencing as-deposited strength, microstructure, and toughness of manual metal arc welds suitable for C-Mn steel fabrications," *International Metals Review*, v.31, No.4, 1986.

Blicharski, M.R., Garcia, C.I., Pytel, S. and DeArdo, A.J., "Structure and Properties of ULCB Plate Steels for Heavy Section Applications," *Processing, Microstructure and Properties of HSLA Steels*, The Minerals, Metals and Materials Society, 1988.

David Taylor Naval Ship Research and Development Center Report, *Pre-Certification Development Plan HSLA 130 Steel For Submarine Construction*, by J.P. Gudas, March 1989.

David Taylor Naval Ship Research and Development Center Report SME-CR-01085, *The Metallurgy of HSLA Steel Weld Metal Produced by the Submerged Arc Process*, by D.K. Matlock and G.R. Edwards, March 1985.

David Taylor Naval Ship Research and Development Center Report SME-CR-07-86, *Development of 100KSI Yield Strength HSLA Steel*, by A.P. Coldren and T.B. Cox, July 1986.

David Taylor Naval Ship Research and Development Center Report SME-88/62, *Physical Properties , Elastic Constants and Metallurgy of HSLA-100 Steel Plate*, by E.J. Czyryca and Richard E. Link, December 1988.

David Taylor Naval Ship Research and Development Center Report SME-CR-06-89, *Influence of Weld Metal Inclusion Type, Content, and Size Distribution on the Microstructure and Properties of High Strength Steel Weld Metal*, by C.W. Ramsay, D.K. Matlock and D.L. Olson, October 1988.

Edmonds, D.V. and Cochrane, R.C., "Structure-Property Relationships in Bainitic Steels," *Metallurgical Transactions A*, v.21A, June 1990.

Grong, O. and Matlock, D.K., "Microstructural development in mild and low-alloy steel weld metals," *International Metals Reviews*, v.31, No.1, 1986.

Grong, O., Siewart, T.A., Martins, G.P. and Olson, D.L., "A Model for the Silicon-Manganese Deoxidation of Steel Weld Metals," *Metallurgical Transactions A*, v.17A, October 1986.

Hertzberg, R.W., *Deformation and Fracture Mechanics of Engineering Materials*, John Wiley and Sons, Inc., 1989.

Irving, R.R., "The Strength in HSLA is the Microalloying," *Iron Age*, November 1987.

Kiessling, R., *Non-metallic Inclusions In Steel*, The Institute of Metals, London, 1989.

Kiessling, R. and Lange, N., *Nonmetallic Inclusions In Steel*, The Metals Society, London, 1978.

Kou, S., *Welding Metallurgy*, John Wiley and Sons, Inc., 1987.

Levin, E.H., Robbins, C.R. and McMurdie, H.F., *Phase Diagrams For Ceramists*, The American Ceramic Society, Inc., 1964.

Pickering, F.B., *Physical Metallurgy and the Design of Steels*, Applied Science Publishers, 1978.

Ricks, R.A., Howell, P.P. and Barritte, G.S., "The nature of acicular ferrite in HSLA steel weld metals," *Journal of Materials Science*, v.17, 1982.

Samuels, L.E., *Optical Microscopy of Carbon Steels*, American Society for Metals, 1980.